

Hierarchical black hole mergers in young, globular and nuclear star clusters: the effect of metallicity, spin and cluster properties

Michela Mapelli¹,^{1,2,3}★ Marco Dall’Amico,^{1,2} Yann Bouffanais,^{1,2} Nicola Giacobbo¹,^{1,2,3,4}
 Manuel Arca Sedda¹,⁵ M. Celeste Artale¹,⁶ Alessandro Ballone¹,^{1,2,3} Ugo N. Di Carlo¹,^{1,2}
 Giuliano Iorio¹,^{1,2,3} Filippo Santoliquido¹,^{1,2} and Stefano Torniamenti^{1,2,3}

¹Physics and Astronomy Department Galileo Galilei, University of Padova, Vicolo dell’Osservatorio 3, I–35122 Padova, Italy

²INFN – Padova, Via Marzolo 8, I–35131 Padova, Italy

³INAF – Osservatorio Astronomico di Padova, Vicolo dell’Osservatorio 5, I–35122, Padova, Italy

⁴School of Physics and Astronomy, Institute for Gravitational Wave Astronomy, University of Birmingham, Birmingham B15 2TT, UK

⁵Astronomisches Rechen-Institut, Zentrum für Astronomie, Universität Heidelberg, Mönchhofstr. 12-14, D-69117 Heidelberg, Germany

⁶Institut für Astro- und Teilchenphysik, Universität Innsbruck, Technikerstrasse 25/8, A-6020 Innsbruck, Austria

Accepted 2021 May 4. Received 2021 April 16; in original form 2021 March 4

ABSTRACT

We explore hierarchical black hole (BH) mergers in nuclear star clusters (NSCs), globular clusters (GCs) and young star clusters (YSCs), accounting for both original and dynamically assembled binary BHs (BBHs). We find that the median mass of both first- and n th-generation dynamical mergers is larger in GCs and YSCs with respect to NSCs because the lighter BHs are ejected by supernova kicks from the lower mass clusters. Also, first- and n th-generation BH masses are strongly affected by the metallicity of the progenitor stars: the median mass of the primary BH of a n th-generation merger is $\sim 24\text{--}38 M_{\odot}$ ($\sim 9\text{--}15 M_{\odot}$) in metal-poor (metal-rich) NSCs. The maximum BH mass mainly depends on the escape velocity: BHs with mass up to several thousand M_{\odot} form in NSCs, while YSCs and GCs host BHs with mass up to several hundred M_{\odot} . Furthermore, we calculate the fraction of mergers with at least one component in the pair-instability mass gap (f_{PI}) and in the intermediate-mass BH regime (f_{IMBH}). In the fiducial model for dynamical BBHs with metallicity $Z = 0.002$, we find $f_{\text{PI}} \approx 0.05, 0.02$ and 0.007 ($f_{\text{IMBH}} \approx 0.01, 0.002$ and 0.001) in NSCs, GCs and YSCs, respectively. Both f_{PI} and f_{IMBH} drop by at least one order of magnitude at solar metallicity. Finally, we investigate the formation of GW190521 by assuming that it is either a nearly equal-mass BBH or an intermediate-mass ratio inspiral.

Key words: black hole physics – gravitational waves – stars: black holes – stars: kinematics and dynamics – galaxies: star clusters: general.

1 INTRODUCTION

The past 5 yr have witnessed the first three observing runs of the Advanced LIGO and Virgo gravitational-wave (GW) interferometers (Aasi et al. 2015; Acernese et al. 2015), leading to the detection of about 50 binary compact object mergers (Abbott et al. 2016a,b,c, 2017, 2019a,b, 2020a,b,c,e,f). Based on the results of independent pipelines, Zackay et al. (2019), Venumadhav et al. (2020) and Nitz et al. (2020) claimed several additional GW candidates. This growing sample represents a Rosetta stone to investigate the formation of binary compact objects.

Among the main results of the third observing run, GW190521 (Abbott et al. 2020d,g) is the most massive binary black hole (BBH) merger observed to date. The primary component mass of GW190521 ($\approx 85 M_{\odot}$) challenges current models of stellar evolution and pair instability (PI) supernovae (e.g. Belczynski et al. 2016b; Spera & Mapelli 2017; Woosley 2017, 2019; Farmer et al. 2019, 2020; Belczynski 2020; Mapelli et al. 2020b; Tanikawa et al. 2020;

Costa et al. 2021; Farrell et al. 2021). Nitz & Capano (2021) proposed a different interpretation for GW190521, as an intermediate-mass ratio inspiral involving an intermediate-mass black hole (IMBH) and an $\sim 16 M_{\odot}$ companion (see also Fishbach & Holz 2020).

Several channels can lead to the formation of BBHs: (i) pairing of primordial black holes (e.g. Carr & Hawking 1974; Bird et al. 2016; Carr, Kühnel & Sandstad 2016; Ali-Haïmoud, Kovetz & Kamionkowski 2017; Scelfo et al. 2018; De Luca et al. 2021a), (ii) binary star evolution through common envelope (e.g. Tutukov & Yungelson 1973; Bethe & Brown 1998; Portegies Zwart & Yungelson 1998; Belczynski, Kalogera & Bulik 2002; Belczynski et al. 2008; Dominik et al. 2013; Eldridge & Stanway 2016; Belczynski et al. 2016a; Mapelli et al. 2017; Stevenson, Berry & Mandel 2017; Klencki et al. 2018; Kruckow et al. 2018; Mapelli & Giacobbo 2018; Eldridge, Stanway & Tang 2019; Mapelli et al. 2019; Neijssel et al. 2019; Spera et al. 2019; Tang et al. 2020) or via homogeneous mixing (e.g. de Mink & Mandel 2016; Mandel & de Mink 2016; Marchant et al. 2016; du Buisson et al. 2020; Riley et al. 2020) and (iii) dynamical processes in triples (e.g. Antonini et al. 2016; Antonini, Toonen & Hamers 2017; Arca-Sedda, Li & Kocsis 2018; Fragione & Loeb 2019; Fragione & Silk 2020; Vigna-Gómez et al. 2021), young

* E-mail: michela.mapelli@unipd.it

star clusters (YSCs; e.g. Banerjee, Baumgardt & Kroupa 2010; Ziosi et al. 2014; Mapelli 2016; Banerjee 2017, 2018, 2021; Di Carlo et al. 2019, 2020b; Kumamoto, Fujii & Tanikawa 2019, 2020), globular clusters (GCs; e.g. Portegies Zwart & McMillan 2000; Downing et al. 2010; Samsing, MacLeod & Ramirez-Ruiz 2014; Rodriguez et al. 2015; Rodriguez, Chatterjee & Rasio 2016a; Askar et al. 2017; Fragione & Kocsis 2018; Rodriguez et al. 2018; Samsing 2018; Roupas & Kazanas 2019; Zevin et al. 2019; Antonini & Gieles 2020b), nuclear star clusters (NSCs; e.g. O’Leary, Kocsis & Loeb 2009; Miller & Lauburg 2009b; Antonini & Rasio 2016; Petrovich & Antonini 2017; Arca-Sedda & Gualandris 2018; Arca Sedda & Benacquista 2019; Rasskazov & Kocsis 2019; Arca Sedda 2020; Arca Sedda et al. 2020) and AGN discs (e.g. McKernan et al. 2012, 2018; Bartos et al. 2017; Stone, Metzger & Haiman 2017; Yang et al. 2019; Tagawa, Haiman & Kocsis 2020).

One of the distinctive signatures of the dynamical scenario is the formation of hierarchical mergers, i.e. repeated mergers of stellar-origin black holes (BHs) that build up more massive ones (Miller & Hamilton 2002; Fishbach, Holz & Farr 2017; Gerosa & Berti 2017; Belczynski & Banerjee 2020; Doctor et al. 2020; Flitter, Muñoz & Kovetz 2020). This process is possible only in dense star clusters, where the merger remnant, which is initially a single BH, can pair up by dynamical exchanges or three-body encounters (e.g. Heggie 1975; Hills & Fullerton 1980). The main obstacle to the formation of second-generation BHs via hierarchical mergers is the relativistic kick that the merger remnant receives at birth (e.g. Fitchett 1983; Favata, Hughes & Holz 2004; Campanelli et al. 2007; Lousto & Zlochower 2011). This kick can be up to several thousand km s^{-1} and can easily eject the BH remnant from its parent star cluster (Holley-Bockelmann et al. 2008; Moody & Sigurdsson 2009; Fragione, Ginsburg & Kocsis 2018; Gerosa & Berti 2019; Arca Sedda et al. 2020). Hence, the interplay between the properties of the host star cluster (e.g. its escape velocity), those of the first-generation BBH population and the magnitude of the kick decides the maximum mass of a merger remnant in a given environment (e.g. Rodriguez et al. 2019; Kimball et al. 2020b).

Due to their high escape velocity ($v_{\text{esc}} \sim 100 \text{ km s}^{-1}$), NSCs are more likely to retain hierarchical mergers than other star clusters (e.g. Antonini & Rasio 2016; Arca-Sedda & Capuzzo-Dolcetta 2019; Yang et al. 2019; Arca Sedda et al. 2020). Antonini, Gieles & Gualandris (2019) find that BH growth becomes substantial for $v_{\text{esc}} > 300 \text{ km s}^{-1}$, leading to the formation of IMBHs (see also Fragione & Silk 2020). Hence, hierarchical mergers can build up IMBHs and also partially fill the PI mass gap between ~ 65 and $\sim 120 M_{\odot}$, explaining the formation of BBHs like GW190521 (e.g. Fragione, Loeb & Rasio 2020b).

One of the main challenges of studying hierarchical mergers is the computational cost. It is nearly impossible to investigate the relevant parameter space with hybrid Monte Carlo and/or N -body simulations of massive star clusters, especially GCs and NSCs. Here, we present a new fast and flexible semianalytic model to investigate hierarchical mergers in different environments, complementary to dynamical simulations. Our new tool allows us to probe the parameter space, including BBH masses, spins, delay times, orbital eccentricities and star cluster properties. With respect to previous semianalytic work (e.g. Choksi et al. 2019; Arca Sedda et al. 2020; Baibhav et al. 2020; Fragione & Silk 2020), our new model fully integrates the evolution of the orbital properties (semimajor axis and eccentricity) by taking into account both GW emission and three-body encounters. Moreover, we consider both original BBHs, i.e. BBHs originating from binary stars, and dynamical BBHs, i.e. BBHs formed by dynamical pairing. Our tool consists in a suite

of PYTHON scripts, dubbed FASTCLUSTER, and is available upon request.

This paper is organized as follows. In Section 2, we lay down the properties of first-generation BBHs. Sections 3 and 4 describe the orbital evolution and the properties of n th-generation BBHs, respectively. Section 5 outlines the relevant star cluster properties. Sections 6 and 7 describe and discuss our main results. Finally, Section 8 is a summary of this paper.

2 FIRST-GENERATION BBHS

In the following analysis, we assume that BBH mergers in star clusters belong to two channels: (i) original binaries, i.e. BBHs that originate from binary stars, and (ii) dynamical binaries, i.e. BBHs that form from three-body encounters. The contribution of original binaries has often been neglected in the past because, in the densest and most massive star clusters, a relevant fraction of the original binaries are ionized before they can form a BBH (e.g. Morscher et al. 2015; Antonini & Rasio 2016). However, especially in low-mass clusters ($\leq 10^4 M_{\odot}$), original binaries can survive and contribute to ≥ 10 per cent of the simulated BBH mergers (e.g. Di Carlo et al. 2019).

2.1 Original binaries

We generate catalogues of mass, semimajor axis and eccentricity of original BBHs with our population-synthesis code¹ MOBSE (Mapelli et al. 2017; Giacobbo, Mapelli & Spera 2018). These catalogues represent the initial properties of our first-generation population. However, the FASTCLUSTER code is extremely flexible and can take its input catalogues from different models, including phenomenological ones.

To build the MOBSE catalogues, we use the same set-up as run $\alpha 5\text{MT}0.5$ in Santoliquido et al. (2021). In particular, we assume a common envelope parameter $\alpha = 5$ and a mass transfer efficiency $f_{\text{MT}} = 0.5$. We adopt the delayed model by Fryer et al. (2012) for core-collapse supernovae, while for (pulsational) PI supernovae, we use the equations reported in the appendix of Mapelli et al. (2020b). This yields a minimum BH mass of $\approx 3 M_{\odot}$ and a maximum BH mass of $\approx 65 M_{\odot}$ from single star evolution (Giacobbo et al. 2018). In tight binary systems, the maximum BH mass is lower ($\approx 45 M_{\odot}$) because the common envelope process removes any residual hydrogen envelope, reducing the final BH mass (Giacobbo & Mapelli 2018).

We draw the zero-age main-sequence mass of the primary stars from a Kroupa (Kroupa 2001) initial mass function. The initial orbital parameters (semimajor axis, orbital eccentricity and mass ratio) of binary stars have been randomly drawn as already described in Santoliquido et al. (2021). In particular, we derive the mass ratio $q = m_2/m_1$ as $\mathcal{F}(q) \propto q^{-0.1}$ with $q \in [0.1, 1]$, the orbital period P from $\mathcal{F}(\Pi) \propto \Pi^{-0.55}$ with $\Pi = \log(P/\text{day}) \in [0.15, 5.5]$ and the eccentricity e from $\mathcal{F}(e) \propto e^{-0.42}$ with $0 \leq e \leq 0.9$ (Sana et al. 2012). To generate our BBH catalogues, we ran 2×10^7 , 10^7 and 10^7 binary stars at metallicity $Z = 0.02$, 0.002 and 0.0002 , respectively. We simulated more binary systems at $Z = 0.02$ because of the lower merger efficiency (e.g. Giacobbo & Mapelli 2018; Klencki et al. 2018). The case with $Z = 0.02$ is approximately the solar metallicity (Anders & Grevesse 1989).

¹MOBSE is publicly available at <http://demoblack.com/>.

Our original BBHs are uniformly sampled from the BBHs that merge within a Hubble time in the MOBSE catalogues. From the MOBSE catalogues, we take the masses of the two BHs, the value of the semimajor axis and that of the orbital eccentricity at the time of the formation of the second BH (t_{form}). We assume that the binary star evolved nearly unperturbed before t_{form} . This is justified by the extremely short orbital period of these binaries (mostly $\leq 50 R_{\odot}$). In a follow-up study, we will integrate the dynamical evolution of the progenitor binary stars inside FASTCLUSTER.

We draw the dimensionless spin magnitudes of the primary and secondary BHs (χ_1 and χ_2) from a Maxwellian distribution with one-dimensional root mean square $\sigma_{\chi} = 0.01, 0.1$ and 0.3 and truncated at $\chi = 1$. $\sigma_{\chi} = 0.1$ is our fiducial case because it is quite reminiscent of the spins inferred from the second GW transient catalogue (GWTC-2, see fig. 10 of Abbott et al. 2020b). We draw the direction of the spins isotropic over the sphere. We make this assumption because even the original BBHs interact with other stars in a star cluster: Even if they do not undergo dynamical exchanges, close encounters should heavily affect their spin orientations (Kumamoto et al. 2021; Trani et al. 2021). For each binary, we also estimate the effective spin (χ_{eff}) and the precessing spin (χ_p), which are defined as follows:

$$\chi_{\text{eff}} = \frac{(m_1 \chi_1 + m_2 \chi_2)}{m_1 + m_2} \cdot \frac{L}{L},$$

$$\chi_p = \frac{c}{B_1 G m_1^2} \max(B_1 S_{1\perp}, B_2 S_{2\perp}), \quad (1)$$

where m_1 (m_2) is the primary (secondary) BH mass, L is the orbital angular momentum of the BBH, c is the speed of light, G is the gravity constant, $B_1 \equiv 2 + 3q/2$ and $B_2 \equiv 2 + 3/(2q)$, with $q = m_2/m_1$. $S_{1\perp}$ and $S_{2\perp}$ are the components of the spin vectors (S_1 and S_2) perpendicular to the orbital angular momentum. Finally $\chi_1 \equiv c S_1/(G m_1^2)$ and $\chi_2 \equiv c S_2/(G m_2^2)$.

An original binary survives in a star cluster only if it is hard, i.e. if its binding energy E_b is larger than the average kinetic energy of a star $\langle E_k \rangle$ (Heggie 1975). Hence, out of all the BBHs calculated with MOBSE, we dynamically evolve only those for which

$$E_b = \frac{G m_1 m_2}{2a} \geq \langle E_k \rangle = \frac{1}{2} m_* \sigma^2, \quad (2)$$

where a is the semimajor axis, m_* is the average mass of a star in the star cluster and σ is the three-dimensional velocity dispersion.

If an original BBH does not satisfy the condition in equation (2), we do not consider it any further. Otherwise, we evolve it by hardening and by GW emission, as described in Section 3.

2.2 Dynamical binaries

Dynamical binaries form either via exchanges between a binary star and an intruder, or via dynamical encounters of three initially single bodies (e.g. Heggie 1975; Hills & Fullerton 1980). The latter are favoured when the fraction of binary systems is small and the local density is extremely high (e.g. during a core collapse), while the former are dominant in star clusters with a large binary fraction, such as YSCs.

The first important requirement for a single BH to pair up with another BH is that it has reached the dense core of the star cluster, where three-body encounters are more likely. This happens over a dynamical friction time-scale (Chandrasekhar 1943):

$$t_{\text{DF}} = \frac{3}{4(2\pi)^{1/2}} \frac{\sigma^3}{G^2 \ln \Lambda} \frac{1}{m_{\text{BH}} \rho}, \quad (3)$$

where m_{BH} is the mass of the BH, σ is the 3D velocity dispersion, ρ is the mass density at the half-mass radius and $\ln \Lambda \sim 10$ is the Coulomb logarithm. After a time t_{DF} , the BH has sunk to the core of the cluster and can acquire a companion by three-body encounters or by exchange.

The time-scale for binary formation via the encounter of three single BHs is (Goodman & Hut 1993; Lee 1995; Fragione & Silk 2020)

$$t_{3\text{bb}} = 125 \text{ Myr} \left(\frac{10^6 \text{ pc}^{-3}}{n_c} \right)^2 \left(\zeta^{-1} \frac{\sigma_{1\text{D}}}{30 \text{ km s}^{-1}} \right)^9 \left(\frac{20 M_{\odot}}{m_{\text{BH}}} \right)^5, \quad (4)$$

where n_c is the central density of the star cluster, $\sigma_{1\text{D}} = \sigma/\sqrt{3}$ is the one-dimensional velocity dispersion at the half-mass radius (assuming isotropic distribution of stellar velocities) and

$$\zeta = \frac{m_* \sigma^2}{m_{\text{BH}} \sigma_{\text{BH}}^2}. \quad (5)$$

In equation (5), σ_{BH} is the velocity dispersion associated with massive BHs of mass m_{BH} . In case of equipartition, $\zeta = 1$. If the system is not in equipartition (i.e. Spitzer instability takes place, Spitzer 1969), then $\zeta < 1$. Here, we assume $\zeta = 1$. The strong dependence of equation (4) on $\sigma_{1\text{D}}$ and m_{BH} makes it critical for the formation of BBHs in dense stellar systems. Here, we use the formalism discussed in O’Leary et al. (2006) and Morscher et al. (2015), which has been adopted in hybrid Monte Carlo simulations and compares well with direct N -body simulations of globular clusters (Rodríguez et al. 2016b).

Finally, the time-scale for the dynamical exchange of a BH into a binary star is (Miller & Lauburg 2009a)

$$t_{12} = 3 \text{ Gyr} \left(\frac{0.01}{f_{\text{bin}}} \right) \left(\frac{10^6 \text{ pc}^{-3}}{n_c} \right) \left(\frac{\sigma}{50 \text{ km s}^{-1}} \right) \times \left(\frac{12 M_{\odot}}{m_{\text{BH}} + 2 m_*} \right) \left(\frac{1 \text{ AU}}{a_{\text{hard}}} \right), \quad (6)$$

where f_{bin} is the binary fraction and $a_{\text{hard}} = G m_*/\sigma^2$ is the minimum semimajor axis of a hard binary system.

We assume that dynamical BBHs form at a time

$$t_{\text{dyn}} = \max\{t_{\text{form}}, [t_{\text{DF}} + \min(t_{3\text{bb}}, t_{12})]\}, \quad (7)$$

where t_{form} is the time for the collapse of the progenitor star to a BH, while t_{DF} , $t_{3\text{bb}}$ and t_{12} are the time-scales defined by equations (3), (4) and (6), respectively. In equation (7), we assume that not only the BH but also its progenitor star undergoes dynamical friction, exchanges and three-body encounters.

In the densest clusters, we should also consider the time-scale t_{cap} for GW two-body captures (e.g. Quinlan & Shapiro 1990):

$$t_{\text{cap}} \sim 7.7 \times 10^3 \text{ Gyr} \left(\frac{M_{\odot}}{m_{\text{BH}}} \right)^2 \left(\frac{10^8 \text{ pc}^{-3}}{n_c} \right) \left(\frac{\sigma}{200 \text{ km s}^{-1}} \right)^{11/7}. \quad (8)$$

However, this time-scale is always longer than $t_{3\text{bb}}$ and t_{12} for all the simulated clusters. Moreover, we also neglect the time-scale for binary–binary encounters which might be even shorter than t_{12} in star clusters with a high binary fraction (e.g. Zevin et al. 2019).

We randomly draw the mass m_1 of the primary BH of first-generation dynamical BBHs from the list of single BHs and BHs in loose binaries in the same MOBSE catalogues as we have described in Section 2.1. BHs from single stars and loose binaries come from the same mass distribution function because only mass transfer and common envelope can affect the final masses in a binary system.

The mass m_2 of the secondary BH is randomly drawn in the interval $[m_{\min}, m_1]$, where $m_{\min} = 3 M_{\odot}$, following the probability distribution function (O’Leary, Meiron & Kocsis 2016):

$$p(m_2) \propto (m_1 + m_2)^4. \quad (9)$$

After generating each mass, we check that both the primary and the secondary BH are not ejected from the star cluster by the supernova kick. We calculate the kick as

$$v_{\text{SN}} = v_{\text{H05}} \frac{\langle m_{\text{NS}} \rangle}{m_{\text{BH}}}, \quad (10)$$

where $\langle m_{\text{NS}} \rangle = 1.33 M_{\odot}$ is the average neutron star mass (Özel & Freire 2016), m_{BH} is the mass of the BH and v_{H05} is a number randomly drawn from a Maxwellian distribution with one-dimensional root mean square $\sigma_V = 265 \text{ km s}^{-1}$. This distribution matches the proper motions of young Galactic pulsars according to the fit by Hobbs et al. (2005) and is adapted to BHs based on linear momentum conservation. If the primary or the secondary BH have $v_{\text{SN}} > v_{\text{esc}}$ (where v_{esc} is the escape velocity from the star cluster), we reject that binary and we draw a new one as detailed above.

We generate the spin magnitude and direction of dynamical BBHs in the same way as those of original BBHs (Section 2.1). We draw the initial eccentricities of dynamical BBHs from the thermal probability distribution $p(e) = 2e$ with $e \in [0, 1)$ (Heggie 1975). The initial semimajor axes follow a distribution $p(a) \propto 1/a$ with $a_{\min} = 1$ and $a_{\max} = 10^3 R_{\odot}$. If the binary generated in this way is soft according to equation (2), we reject the value of a and we generate a new value. In this way, all the dynamical binaries are initially hard binaries. We then evolve each dynamical binary as described in Section 3.

3 ORBITAL EVOLUTION

After their formation, both original and dynamical BBHs undergo binary-single encounters, i.e. close Newtonian gravitational encounters with single stars or BHs in the star cluster. A hard binary hardens by binary-single encounters, i.e. its semimajor axis decreases at a rate (Heggie 1975)

$$\frac{da}{dt} = -2\pi\xi \frac{G\rho_c}{\sigma} a^2, \quad (11)$$

where ρ_c is the core mass density and $\xi \sim 0.1\text{--}10$ is a numerically calibrated constant (Hills 1983). Quinlan (1996) find $\xi \approx 3$, while Miller & Hamilton (2002) and Sesana, Haardt & Madau (2006) obtain $\xi \approx 0.2\text{--}3$. In the following, we adopt $\xi = 3$.

Dynamical encounters also affect the orbital eccentricity e . Following Quinlan (1996), we define the parameter

$$\kappa \equiv \frac{de}{d \ln(1/a)}. \quad (12)$$

Hence, the variation of eccentricity because of dynamical hardening can be expressed as

$$\frac{de}{dt} = 2\pi\xi\kappa \frac{G\rho_c}{\sigma} a. \quad (13)$$

The values of κ have been calibrated via N -body encounters (Quinlan 1996; Sesana et al. 2006), yielding values $\kappa \sim 0.01\text{--}0.1$. Here, we adopt $\kappa = 0.1$ because large values of κ better describe the case in which the ratio between the mass of the BBH and the mass of the intruder is close to 1.

At the same time, a BBH evolves by GW emission, which shrinks the orbit and circularizes it. According to Peters (1964), shrinking

and circularization by GW emission are described as

$$\begin{aligned} \frac{da}{dt} &= -\frac{64}{5} \frac{G^3 m_1 m_2 (m_1 + m_2)}{c^5 a^3 (1 - e^2)^{7/2}} f_1(e) \\ \frac{de}{dt} &= -\frac{304}{15} e \frac{G^3 m_1 m_2 (m_1 + m_2)}{c^5 a^4 (1 - e^2)^{5/2}} f_2(e), \end{aligned} \quad (14)$$

where

$$\begin{aligned} f_1(e) &= \left(1 + \frac{73}{24} e^2 + \frac{37}{96} e^4\right) \\ f_2(e) &= \left(1 + \frac{121}{304} e^2\right). \end{aligned} \quad (15)$$

Putting together equations (11), (13) and (14), we can describe the evolution of a binary under the combined effect of dynamical hardening and GW emission as (Mapelli 2018)

$$\begin{aligned} \frac{da}{dt} &= -2\pi\xi \frac{G\rho_c}{\sigma} a^2 - \frac{64}{5} \frac{G^3 m_1 m_2 (m_1 + m_2)}{c^5 a^3 (1 - e^2)^{7/2}} f_1(e), \\ \frac{de}{dt} &= 2\pi\xi\kappa \frac{G\rho_c}{\sigma} a - \frac{304}{15} e \frac{G^3 m_1 m_2 (m_1 + m_2)}{c^5 a^4 (1 - e^2)^{5/2}} f_2(e). \end{aligned} \quad (16)$$

FASTCLUSTER performs the above integration with the Euler scheme and an adaptive time-step. In particular, we reduce (increase) the time-step by a factor of 10 (2) whenever the percentage change of a between two time-steps is >1 per cent (≤ 0.1 per cent). The code also includes a Runge–Kutta fourth-order integrator, if higher accuracy is needed.

For each original binary, we start the integration described by equations (16) after the second BH has formed, i.e. after a time t_{form} . For each first-generation dynamical binary, we start the integration after the binary has formed by dynamical encounters, i.e. after the time t_{dyn} described by equation (7). We integrate each binary (original or dynamical) for a time equal to $\min(t_{\text{merg}}, t_{\text{Hubble}})$, where $t_{\text{Hubble}} \approx 13.6 \text{ Gyr}$ is the Hubble time. For original binaries, $t_{\text{merg}} = t_{\text{form}} + t_{\text{del}}$, where t_{del} is the delay time between the formation of the BBH and its merger. For first-generation dynamical binaries, $t_{\text{merg}} = t_{\text{dyn}} + t_{\text{del}}$. We assume that the binary merges when $a \leq r_{\text{ISCO}}$, where r_{ISCO} is the radius of the innermost stable circular orbit.

At each time-step, we compare the current time t with the lifetime of the host star cluster (t_{SC}). If $t \leq t_{\text{SC}}$, the binary is integrated according to equations (16). If $t > t_{\text{SC}}$, the binary no longer hardens and is integrated according to equations (14).

At the beginning of the integration of equations (16), we also compare the maximum semimajor axis for ejection by three-body encounters (Miller & Hamilton 2002):

$$a_{\text{ej}} = \frac{2\xi m_*^2}{(m_1 + m_2)^3} \frac{G m_1 m_2}{v_{\text{esc}}^2}, \quad (17)$$

with the maximum semimajor axis for which shrinking by GW emission becomes dominant over shrinking by dynamical hardening (e.g. equation 23 of Baibhav et al. 2020):

$$a_{\text{GW}} = \left[\frac{32 G^2}{5 \pi \xi c^5} \frac{\sigma m_1 m_2 (m_1 + m_2)}{\rho_c (1 - e^2)^{7/2}} f_1(e) \right]^{1/5}. \quad (18)$$

If $a_{\text{ej}} < a_{\text{GW}}$, the binary evolves inside the cluster as described by equations (16), until it merges or the star cluster dies by evaporation ($t > t_{\text{SC}}$). If the star cluster evaporates before the binary has merged, we keep integrating the orbital evolution of the binary by GW emission, following equations (14), up to $\min(t_{\text{merg}}, t_{\text{Hubble}})$.

If $a_{\text{ej}} \geq a_{\text{GW}}$, the binary is ejected from the cluster by dynamical recoil before it merges. Inside the main loop of the integration, we switch from equations (16) (dynamical hardening plus GW emission)

to equations (14) (GW emission only) either when the star cluster evaporates ($t > t_{\text{SC}}$) or when the current semimajor axis of the binary $a(t) \leq a_{\text{ej}}$ (whichever happens first).

This integration is a significant improvement with respect to previous work, which is based on order of magnitude time-scales. On the other hand, it still contains several approximations. For example, we neglect dynamical exchanges, which might change the masses of the binary system.

When a binary merges, we model the mass and spin of the merger remnant using fitting formulas from numerical relativity, as described by Jiménez-Forteza et al. (2017) (see also Rezzolla et al. 2008; Hofmann, Barausse & Rezzolla 2016). The final mass is ≈ 0.9 the total mass of the two merging BHs, while the final spin magnitude clusters around $\chi_f \approx 0.7\text{--}0.9$.

4 NTH GENERATIONS

4.1 Relativistic kicks

At coalescence, the merger product receives a kick because of the transfer of linear momentum caused by asymmetries in GW emission (Fitchett 1983; Lousto et al. 2012; Maggiore 2018). We model the magnitude of relativistic kicks following Lousto et al. (2012):

$$v_{\text{kick}} = (v_m^2 + v_{\perp}^2 + 2 v_m v_{\perp} \cos \phi + v_{\parallel}^2)^{1/2}, \quad (19)$$

where

$$\begin{aligned} v_m &= A \eta^2 \frac{(1-q)}{(1+q)} (1+B\eta), \\ v_{\perp} &= H \frac{\eta^2}{(1+q)} |\chi_{1\parallel} - q \chi_{2\parallel}|, \\ v_{\parallel} &= \frac{16\eta^2}{(1+q)} [V_{1,1} + V_A S_{\parallel} + V_B S_{\parallel}^2 + V_C S_{\parallel}^3] \\ &\quad \times |\chi_{1\perp} - q \chi_{2\perp}| \cos(\phi_{\Delta} - \phi). \end{aligned} \quad (20)$$

In the above equations, $q = m_2/m_1$ with $m_2 \leq m_1$, $\eta = q(1+q)^{-2}$, $A = 1.2 \times 10^4 \text{ km s}^{-1}$, $B = -0.93$, $H = 6.9 \times 10^3 \text{ km s}^{-1}$, $(V_{1,1}, V_A, V_B, V_C) = (3678, 2481, 1792, 1506) \text{ km s}^{-1}$, while χ_1 and χ_2 are the dimensionless spin vectors of the primary and secondary BHs, respectively. Moreover, $\chi_{1\parallel}$ ($\chi_{2\parallel}$) is the component of the spin of the primary (secondary) BH parallel to the orbital angular momentum of the binary system, while $\chi_{1\perp}$ ($\chi_{2\perp}$) is the component of the spin of the primary (secondary) BH lying in the orbital plane. S_{\parallel} is the component parallel to the orbital angular momentum of the vector $\mathbf{S} = 2(\chi_1 + q^2 \chi_2)/(1+q)^2$. Finally, ϕ_{Δ} represents the angle between the direction of the infall at merger (which we randomly draw in the BBH orbital plane) and the in-plane component of $\Delta \equiv (m_1 + m_2)^2 (\chi_1 - q \chi_2)/(1+q)$, while ϕ is the phase of the BBH, randomly drawn between 0 and 2π .

If $v_{\text{kick}} < v_{\text{esc}}$, the merger product is retained in the star cluster, otherwise it is ejected. If it is ejected, it cannot acquire a new companion by three-body encounters: we do not consider it for the next generations.

4.2 Relevant time-scales and orbital properties

Even if $v_{\text{kick}} < v_{\text{esc}}$, the merger remnant is a single BH at birth and it is likely ejected into the outskirts of the star cluster by the relativistic kick. It must sink back to the dense central regions of the star cluster by dynamical friction, before it can acquire a new companion dynamically. Hence, for each merger remnant still bound to the cluster, we first calculate the dynamical friction time-scale

according to equation (3). From now on, there is no difference in the treatment between remnants that originated from the merger of an original BBH or a dynamical BBH.

After a time t_{DF} , the BH is back to the core of the cluster and can acquire a new companion by three-body encounter or by exchange. We then calculate the time needed for the merger remnant to form a new binary with another BH as the minimum between $t_{3\text{bb}}$ (equation 4) and t_{12} (equation 6).

The total time to form a second-generation BBH is then

$$t_{\text{dyn, ng}} = t_{\text{merg}} + t_{\text{DF}} + \min(t_{3\text{bb}}, t_{12}), \quad (21)$$

where t_{merg} is the time to form and merge the previous generation BBH, as described in the previous sections. If $t_{\text{dyn, ng}} < \min(t_{\text{SC}}, t_{\text{Hubble}})$, the second- (or n th-) generation BBH can form. We then draw the secondary mass according to equation (9) and the new eccentricity and semimajor axis as detailed in Section 2.2. The spin of the secondary component is drawn from the distribution of first-generation (n th-generation) BHs if the mass of the secondary is lower (higher) than the maximum mass of first-generation BHs.

We then integrate the evolution of the orbital properties of the n th-generation binary as described in Section 3, until the minimum between the Hubble time and the merger time t_{merg} of the new binary, which now includes not only the formation time of the binary but also the time-span of the previous generations. If the n th-generation binary merges, we calculate the properties of the merger remnant and the relativistic kick and we re-start the loop from Section 4.1.

It might be useful to summarize here the relevant time-scales used in FASTCLUSTER and how they work:

- (i) For dynamical (original) binaries, t_{form} is the time elapsed between the formation of the progenitor star (binary star) and the formation of the BH (BBH).
- (ii) Equation (3) defines the dynamical friction time-scale t_{DF} .
- (iii) For first-generation dynamical binaries and for all n th-generation binaries, $t_{3\text{bb}}$, defined in equation (4), is the time-scale for the formation of a BBH by three-body encounters.
- (iv) For first-generation dynamical binaries and for all n th-generation binaries, t_{12} , defined in equation (6), is the time-scale for the formation of a BBH by dynamical exchange.
- (v) t_{dyn} is the total time required to form a first-generation dynamical BBH (equation 7).
- (vi) $t_{\text{dyn, ng}}$ is the total time required to form a n th-generation BBH (equation 21), including the assembly and evolution of previous generations.
- (vii) We define t_{del} as the time elapsed between the formation of the BBH (via either binary evolution or dynamical interactions) and its merger by GW emission. During this time a binary is evolved according to equations (16) if it is still inside the star cluster and according to equations (14) after its dynamical ejection or after the evaporation of the star cluster.
- (viii) We define t_{merg} as the total time elapsed from the beginning of the simulation to the merger of a BBH. For n th-generation BBHs, $t_{\text{merg, ng}}$ includes the evolutionary times of the previous generations.
- (ix) We indicate the Hubble time as t_{Hubble} .
- (x) The lifetime of the star cluster is t_{SC} .

5 STAR CLUSTER PROPERTIES

Most of the aforementioned equations depend on the properties of the host star cluster. Here we assume, for the sake of simplicity, that the star cluster properties do not evolve in time. We will add the

evolution of the star cluster in a follow-up study. We consider three different flavours of star clusters: NSCs, GCs and YSCs.

Each star cluster is uniquely defined by its lifetime t_{SC} , total mass M_{tot} , binary fraction f_{bin} and half-mass density ρ . We assume $t_{\text{SC}} = 13.6, 12$ and 1 Gyr for NSCs, GCs (Gratton et al. 1997, 2003; VandenBerg et al. 2013) and YSCs (Portegies Zwart, McMillan & Gieles 2010), respectively. Furthermore, we assume $f_{\text{bin}} = 0.01, 0.1$ and 1 in NSCs (Antonini & Rasio 2016), GCs (Ji & Bregman 2015) and YSCs (Sana et al. 2012), respectively. We draw the total masses from a lognormal distribution with mean $\langle \log_{10} M_{\text{tot}}/M_{\odot} \rangle = 6.18, 5.3$ and 4.3 for NSCs, GCs and YSCs, respectively. We assume a fiducial standard deviation $\sigma_M = 0.4$ for all star cluster flavours. We also consider the cases in which $\sigma_M = 0.2$ and 0.6 . We draw the density at the half-mass radius from a lognormal distribution with mean $\langle \log_{10} \rho/(M_{\odot} \text{pc}^{-3}) \rangle = 5, 3.3$ and 3.3 for NSCs, GCs and YSCs, respectively. We assume a fiducial standard deviation $\sigma_{\rho} = 0.4$ for all star cluster flavours. The values of M_{tot} and ρ are inferred from the observations reported in Neumayer, Seth & Böker (2020) for NSCs and GCs (see also Harris 1996; Georgiev et al. 2016) and from Portegies Zwart et al. (2010) for YSCs. For each star cluster, we assume a core density $\rho_c = 20 \rho$. We derive the escape velocity from M_{tot} and ρ (Georgiev et al. 2009a,b; Fragione & Silk 2020) using the following relationship:

$$v_{\text{esc}} = 40 \text{ km s}^{-1} \left(\frac{M_{\text{tot}}}{10^5 M_{\odot}} \right)^{1/3} \left(\frac{\rho}{10^5 M_{\odot} \text{pc}^{-3}} \right)^{1/6}. \quad (22)$$

Equation (22) results in a distribution of escape velocities fairly consistent with the observational sample reported in fig. 1 of Antonini & Rasio (2016) for GCs and NSCs.

Here, we do not consider NSCs that host a supermassive BH (SMBH). In such clusters, most of the binaries inside the influence radius of the SMBH are soft and are disrupted over a time-scale (Binney & Tremaine 1987):

$$t_{\text{ev}} = \frac{(m_1 + m_2) \sigma}{16 \sqrt{\pi} G m_* \rho_c a \ln \Lambda}. \quad (23)$$

We refer to Arca Sedda (2020) for a detailed treatment of this case.

6 RESULTS

6.1 Description of runs

We ran 42 different realizations of our models, half of them for original binaries and the other half for dynamical binaries, playing with the most relevant parameters. We consider three different families of star clusters (NSCs, GCs and YSCs), three different metallicities $Z = 0.0002, 0.002$ and 0.02 (roughly corresponding to $0.01, 0.1$ and $1 Z_{\odot}$), three different values of the spin magnitude parameter $\sigma_{\chi} = 0.01, 0.1$ and 0.3 and three different values of $\sigma_M = 0.2, 0.4$ and 0.6 . Table 1 summarizes the details of each model. Each model consists of 10^6 first-generation BBHs. In the following section, we describe the main results of these runs.

6.2 Dynamical binaries in NSCs, GCs and YSCs

Figs 1–3 show the main properties of dynamical BBHs formed in NSCs, GCs and YSCs, respectively, according to our fiducial models (NSC.D1, GC.D1 and YSC.D1). Only BBHs that merge within a Hubble time are shown, both first and n th generation. This figure does not distinguish between BBHs that merge inside or outside their parent star cluster.

Table 1. Summary of the models.

Model	Formation	Star cluster	Z	σ_{χ}	σ_M
NSC.D1	Dynamical	NSC	0.002	0.1	0.4
NSC.D2	Dynamical	NSC	0.0002	0.1	0.4
NSC.D3	Dynamical	NSC	0.02	0.1	0.4
NSC.D4	Dynamical	NSC	0.002	0.01	0.4
NSC.D5	Dynamical	NSC	0.002	0.3	0.4
NSC.D6	Dynamical	NSC	0.002	0.1	0.2
NSC.D7	Dynamical	NSC	0.002	0.1	0.6
GC.D1	Dynamical	GC	0.002	0.1	0.4
GC.D2	Dynamical	GC	0.0002	0.1	0.4
GC.D3	Dynamical	GC	0.02	0.1	0.4
GC.D4	Dynamical	GC	0.002	0.01	0.4
GC.D5	Dynamical	GC	0.002	0.3	0.4
GC.D6	Dynamical	GC	0.002	0.1	0.2
GC.D7	Dynamical	GC	0.002	0.1	0.6
YSC.D1	Dynamical	YSC	0.002	0.1	0.4
YSC.D2	Dynamical	YSC	0.0002	0.1	0.4
YSC.D3	Dynamical	YSC	0.02	0.1	0.4
YSC.D4	Dynamical	YSC	0.002	0.01	0.4
YSC.D5	Dynamical	YSC	0.002	0.3	0.4
YSC.D6	Dynamical	YSC	0.002	0.1	0.2
YSC.D7	Dynamical	YSC	0.002	0.1	0.6
NSC.O1	Original	NSC	0.002	0.1	0.4
NSC.O2	Original	NSC	0.0002	0.1	0.4
NSC.O3	Original	NSC	0.02	0.1	0.4
NSC.O4	Original	NSC	0.002	0.01	0.4
NSC.O5	Original	NSC	0.002	0.3	0.4
NSC.O6	Original	NSC	0.002	0.1	0.2
NSC.O7	Original	NSC	0.002	0.1	0.6
GC.O1	Original	GC	0.002	0.1	0.4
GC.O2	Original	GC	0.0002	0.1	0.4
GC.O3	Original	GC	0.02	0.1	0.4
GC.O4	Original	GC	0.002	0.01	0.4
GC.O5	Original	GC	0.002	0.3	0.4
GC.O6	Original	GC	0.002	0.1	0.2
GC.O7	Original	GC	0.002	0.1	0.6
YSC.O1	Original	YSC	0.002	0.1	0.4
YSC.O2	Original	YSC	0.0002	0.1	0.4
YSC.O3	Original	YSC	0.02	0.1	0.4
YSC.O4	Original	YSC	0.002	0.01	0.4
YSC.O5	Original	YSC	0.002	0.3	0.4
YSC.O6	Original	YSC	0.002	0.1	0.2
YSC.O7	Original	YSC	0.002	0.1	0.6

Notes. Column 1: name of the model (NSC.D1, GC.D1 and YSC.D1 are our fiducial models for dynamical binaries, while NSC.O1, GC.O1 and YSC.O1 are our fiducial models for original binaries); column 2: formation path of the binary (original or dynamical); column 3: star cluster type (NSC, GC, YSC); column 4: metallicity of first-generation BHs ($Z = 0.0002, 0.002, 0.02$); column 5: root mean square value of the Maxwellian distribution of spin magnitudes ($\sigma_{\chi} = 0.01, 0.1, 0.3$); column 6: standard deviation of the lognormal distribution of total star cluster masses ($\sigma_M = 0.2, 0.4, 0.6$).

The mass function of first-generation BBHs is similar in NSCs, GCs and YSCs because it comes from the same catalogues, but for one crucial difference: The assumption that only BHs receiving a natal kick lower than the escape velocity have a chance to pair up dynamically (Section 2.2) prevents the formation of low-mass BBHs especially in the clusters with the lowest escape velocity. Hence, NSCs witness the formation of more low-mass BBHs than both GCs and YSCs. For this reason, the mass function of first- and n th-generation dynamical BBHs includes a larger fraction of low-mass systems ($m_1 < 20 M_{\odot}$) in NSCs than in both GCs and YSCs (see also Table 2).

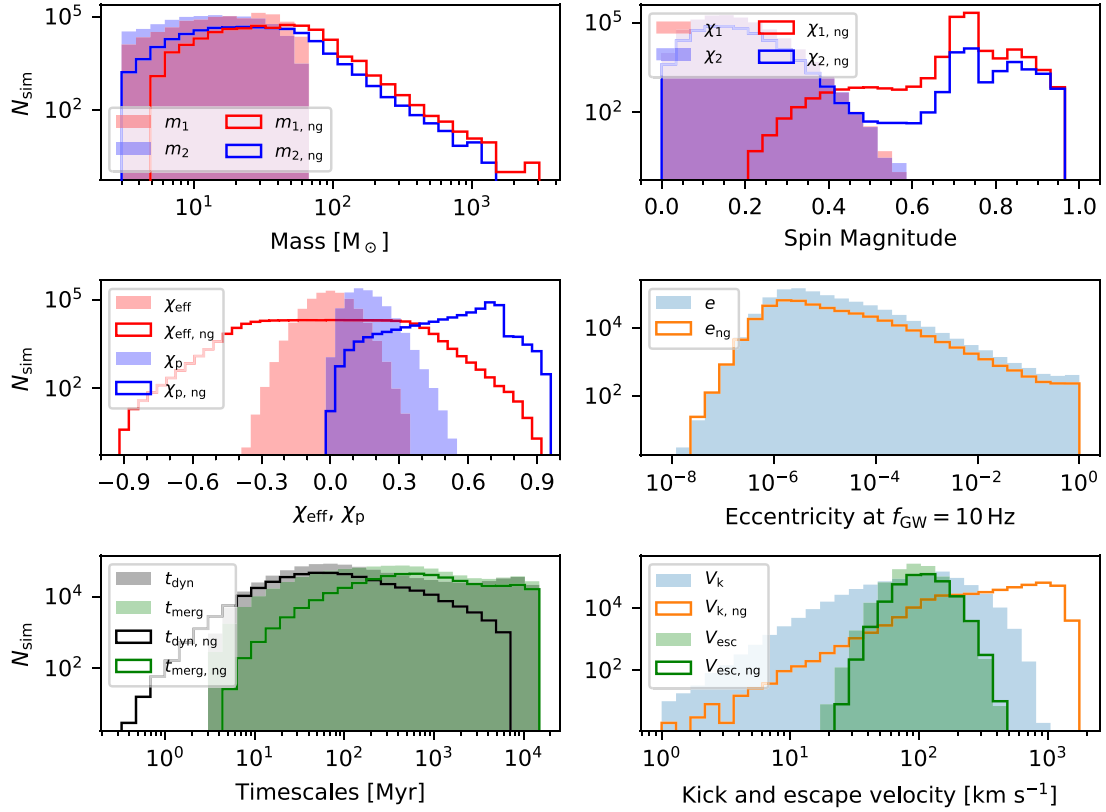


Figure 1. Main properties of dynamical BBH mergers in NSCs, according to our fiducial model (NSC.D1). The upper left-hand panel shows the relevant masses. Filled red (blue) histogram: mass of the primary, m_1 (secondary, m_2), in first-generation mergers; unfilled red (blue) histogram: mass of the primary, $m_{1,ng}$ (secondary, $m_{2,ng}$) in n th-generation mergers. The upper right-hand panel shows the dimensionless spin parameters. Filled red (blue) histogram: dimensionless spin of the primary, χ_1 (secondary, χ_2) in first-generation mergers; unfilled red (blue) histogram: dimensionless spin of the primary, $\chi_{1,ng}$ (secondary, $\chi_{2,ng}$) in n th-generation mergers. The middle left-hand panel shows the effective and precessing spin parameters. Filled red (blue) histogram: effective (precessing) spin χ_{eff} (χ_p) in first-generation mergers; unfilled red (blue) histogram: effective (precessing) spin $\chi_{\text{eff},ng}$ ($\chi_{p,ng}$) in n th-generation mergers. In the middle right-hand panel, filled light-blue (unfilled orange) histogram: orbital eccentricity when the GW frequency $f_{\text{GW}} = 10$ Hz for first-generation (n th-generation) mergers. In the lower left-hand panel, we show the most important time-scales. Gray filled histogram: time for the dynamical formation of first-generation BBHs (t_{dyn} , equation 7); green filled histogram: delay time for the merger of the first-generation BBHs (t_{merge}); black unfilled histogram: time for the dynamical formation of n th-generation BBHs ($t_{\text{dyn},ng}$, equation 21); green unfilled histogram: delay time for the merger of the n th-generation BBHs ($t_{\text{merge},ng}$). The lower right-hand panel shows the most important velocities. Light-blue filled histogram: relativistic kick velocity received by the merger product of the first-generation BBHs (V_k); orange unfilled histogram: relativistic kick velocity received by the merger product of the n th-generation BBHs ($V_{k,ng}$); green filled histogram: escape velocity of the star clusters that host the first-generation BBH mergers (V_{esc}); green unfilled histogram: escape velocity of the star clusters that host the n th-generation BBH mergers ($V_{\text{esc},ng}$). The y-axis of all the histograms shows the number of simulated BHs N_{sim} , without normalization.

The mass function of n th-generation BBHs peaks at values ~ 30 – $100 M_{\odot}$ in all considered star clusters, indicating that most n th-generation BBHs are just second generation. The main difference between NSCs, GCs and YSCs is the maximum mass of n th-generation BBHs. NSCs, because of their high escape velocity, allow a larger number of generations to form, up to primary masses in excess of $\sim 10^3 M_{\odot}$ (Table 2). The main limitation to build even more massive BHs in NSCs is represented by the long time-scales: After ≈ 10 generations at most, the simulation reaches the Hubble time. In contrast, the maximum masses in both GCs and YSCs are a few times $10^2 M_{\odot}$. Another crucial difference between NSCs and either GCs or YSCs is the fraction of n th- to first-generation mergers (Table 2).

The distribution of spins looks similar in NSCs, GCs and YSCs, by construction, because we assume the same spin models. The main feature is the double horned distribution of the precessing spin χ_p :

Most first-generation mergers have precessing spin squeezed toward low values (~ 0.1 – 0.2), while n th-generation mergers tend to have high values of $\chi_p \sim 0.7$. This creates a sort of spin gap between ~ 0.3 and ~ 0.6 , as already discussed in Baibhav et al. (2020) and Fishbach & Holz (2020). The importance of the secondary peak at large χ_p with respect to the primary peak at $\chi_p \sim 0.1$ – 0.2 depends on the fraction of n th- to first-generation mergers.

The eccentricity distributions when the binary enters the LIGO–Virgo band (i.e. when the frequency of GW emission is $f_{\text{GW}} = 10$ Hz) are similar for NSCs, GCs and YSCs because the dynamical evolution is comparable for the three samples. The fraction of dynamical BBHs with eccentricity $e > 0.1$ ($e > 0.9$) at $f_{\text{GW}} = 10$ Hz is $\sim 2 \times 10^{-3}$ ($\sim 10^{-4}$) for all types of star clusters, when accounting for both first- and n th-generation mergers (Table 2).

Finally, the dynamical formation time-scales of first- and n th-generation dynamical BBHs (t_{dyn} and $t_{\text{dyn},ng}$) are clearly squeezed

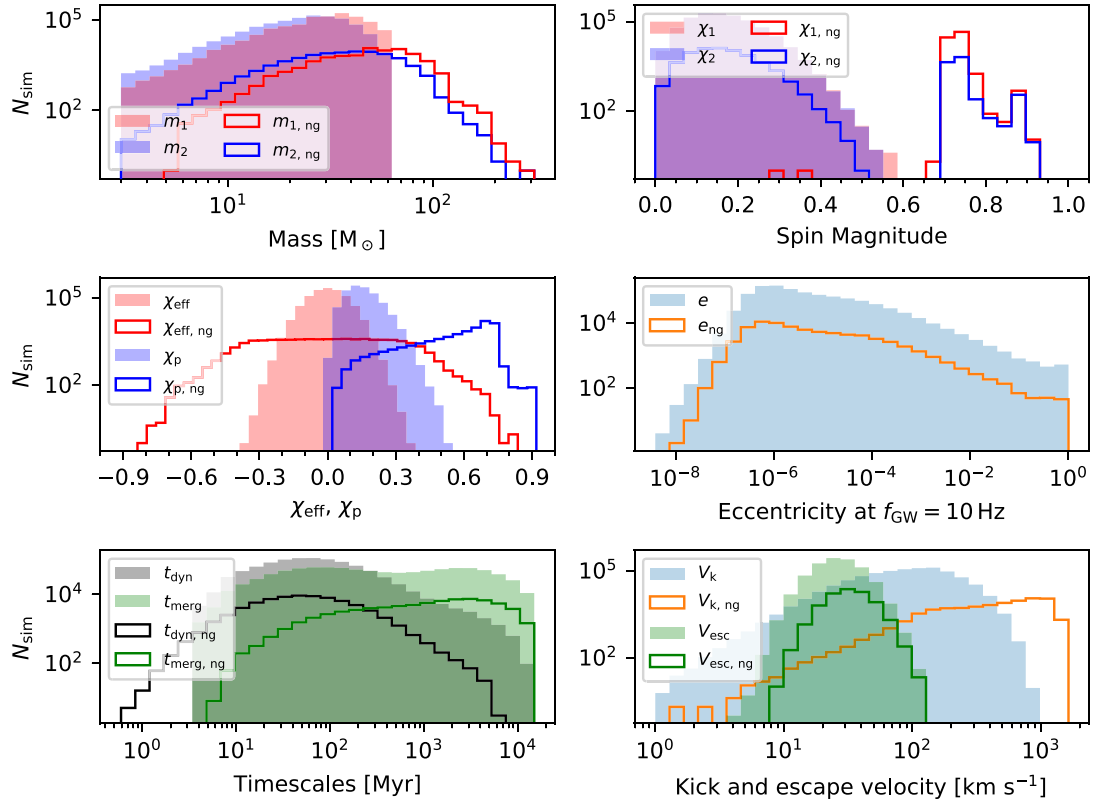


Figure 2. Same as Fig. 1, but for GCs, according to our fiducial model (GC.D1).

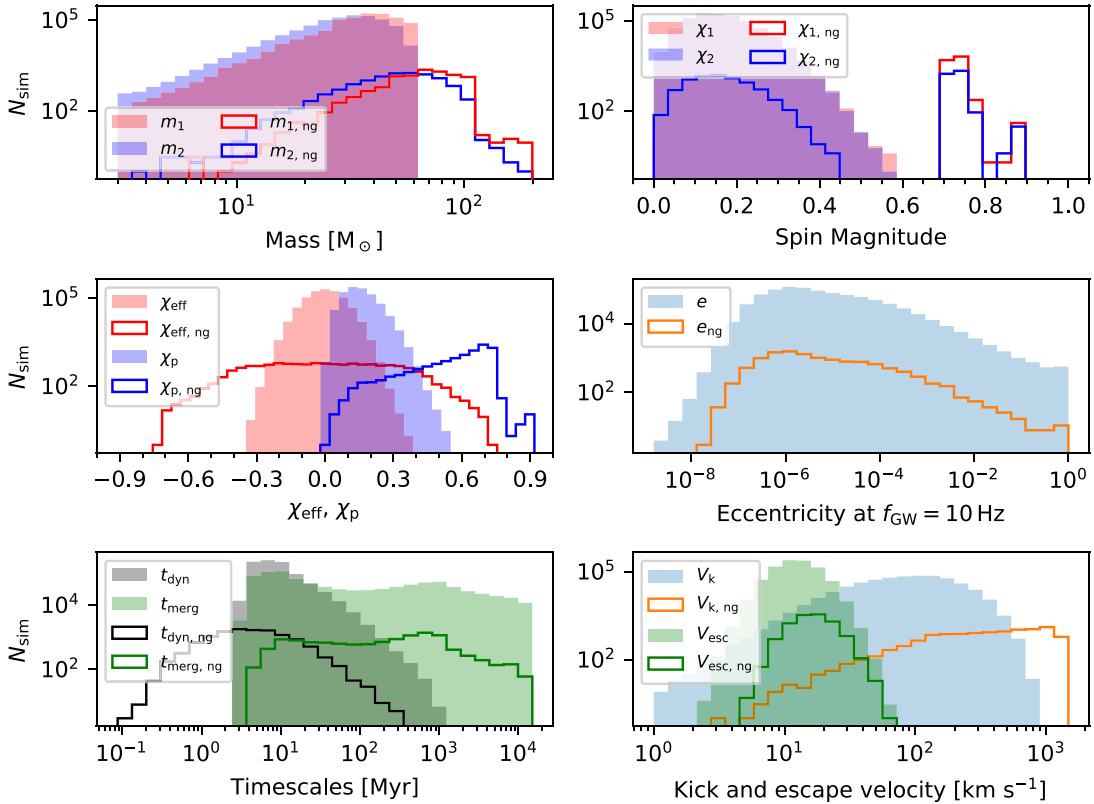


Figure 3. Same as Fig. 1, but for YSCs, according to our fiducial model (YSC.D1).

Table 2. Main results of the models presented in this paper.

Model	f_{ng}	f_{PI}	f_{IMBH}	Med m_1 (M_{\odot})	Med $m_{1,\text{ng}}$ (M_{\odot})	Max $m_{1,\text{ng}}$ (M_{\odot})	N_g	$f(e > 0.1)$	$f(e > 0.9)$	f_{GW190521} LVC	f_{GW190521} Nitz and Capano
NSC_D1	0.318	0.048	0.012	19	34	3040	10	0.002	9×10^{-5}	0.019	4×10^{-4}
NSC_D2	0.319	0.066	0.021	20	35	28 390	15	0.002	8×10^{-5}	0.014	2×10^{-4}
NSC_D3	0.308	0.003	7×10^{-4}	8	15	1092	10	0.001	6×10^{-5}	6×10^{-4}	8×10^{-6}
NSC_D4	0.414	0.064	0.015	19	34	2742	10	0.002	8×10^{-5}	0.019	3×10^{-4}
NSC_D5	0.174	0.026	0.006	19	35	3312	11	0.002	8×10^{-5}	0.007	10^{-4}
NSC_D6	0.321	0.044	0.009	18	30	1486	8	0.002	9×10^{-5}	0.013	2×10^{-4}
NSC_D7	0.312	0.053	0.015	21	38	43 587	17	0.002	7×10^{-5}	0.015	2×10^{-4}
GC_D1	0.073	0.021	0.002	31	51	302	4	0.002	9×10^{-5}	0.008	10^{-4}
GC_D2	0.072	0.026	0.006	35	58	341	4	0.002	9×10^{-5}	0.006	2×10^{-5}
GC_D3	0.077	5×10^{-4}	2×10^{-5}	17	31	164	4	0.002	8×10^{-5}	10^{-4}	0
GC_D4	0.228	0.075	0.009	31	53	343	5	0.002	9×10^{-5}	0.024	10^{-4}
GC_D5	0.015	0.004	4×10^{-4}	31	49	197	4	0.002	10^{-4}	0.001	3×10^{-6}
GC_D6	0.069	0.021	0.002	31	52	278	4	0.002	9×10^{-5}	0.007	2×10^{-5}
GC_D7	0.078	0.022	0.003	32	50	426	5	0.002	9×10^{-5}	0.007	3×10^{-5}
YSC_D1	0.013	0.007	0.001	38	69	189	3	0.002	10^{-4}	0.003	4×10^{-5}
YSC_D2	0.013	0.008	0.003	42	76	226	3	0.002	10^{-4}	0.003	3×10^{-6}
YSC_D3	0.009	3×10^{-5}	0.0	19	37	86	3	0.002	9×10^{-5}	10^{-5}	0
YSC_D4	0.096	0.059	0.010	38	71	293	4	0.002	10^{-4}	0.021	5×10^{-5}
YSC_D5	0.002	0.001	10^{-4}	38	66	147	3	0.002	10^{-4}	0.003	0
YSC_D6	0.011	0.007	0.001	38	71	238	4	0.002	10^{-4}	0.002	5×10^{-6}
YSC_D7	0.015	0.008	0.001	38	65	319	4	0.002	10^{-4}	0.003	10^{-5}
NSC_O1	0.305	0.017	0.005	9	29	1783	10	6×10^{-4}	10^{-4}	0.003	3×10^{-5}
NSC_O2	0.332	0.012	0.002	10	24	2903	10	6×10^{-4}	4×10^{-5}	0.002	9×10^{-5}
NSC_O3	0.243	3×10^{-4}	10^{-4}	6	9	751	10	0.014	0.014	6×10^{-5}	3×10^{-6}
NSC_O4	0.396	0.022	0.007	9	30	4784	12	8×10^{-4}	10^{-4}	0.003	10^{-4}
NSC_O5	0.164	0.008	0.003	9	26	1546	9	4×10^{-4}	10^{-4}	0.001	6×10^{-5}
NSC_O6	0.320	0.015	0.004	9	26	1285	9	7×10^{-4}	10^{-4}	0.002	9×10^{-5}
NSC_O7	0.287	0.019	0.008	9	32	11 796	13	6×10^{-4}	10^{-4}	0.003	10^{-4}
GC_O1	0.053	0.003	2×10^{-4}	9	40	225	4	10^{-4}	3×10^{-5}	9×10^{-4}	10^{-6}
GC_O2	0.044	0.003	4×10^{-5}	10	31	203	4	10^{-4}	3×10^{-5}	2×10^{-4}	3×10^{-6}
GC_O3	0.020	10^{-6}	0.0	6	8	68	4	0.018	0.018	0	0
GC_O4	0.174	0.010	6×10^{-4}	9	41	236	5	4×10^{-4}	3×10^{-5}	6×10^{-4}	2×10^{-5}
GC_O5	0.011	5×10^{-4}	3×10^{-5}	9	39	149	4	3×10^{-5}	8×10^{-6}	2×10^{-5}	2×10^{-6}
GC_O6	0.048	0.003	2×10^{-4}	9	41	213	4	10^{-4}	10^{-5}	10^{-4}	10^{-6}
GC_O7	0.058	0.003	3×10^{-4}	9	39	308	6	10^{-4}	10^{-5}	2×10^{-4}	8×10^{-6}
YSC_O1	0.001	10^{-4}	0.0	9	53	99	3	2×10^{-5}	2×10^{-5}	4×10^{-5}	0
YSC_O2	7×10^{-4}	10^{-4}	0.0	10	41	85	3	3×10^{-5}	3×10^{-5}	4×10^{-6}	0
YSC_O3	0.002	0.0	0.0	6	8	21	3	0.022	0.022	0	0
YSC_O4	0.007	10^{-4}	3×10^{-5}	9	54	124	3	7×10^{-5}	5×10^{-5}	3×10^{-5}	10^{-6}
YSC_O5	2×10^{-4}	2×10^{-5}	2×10^{-6}	9	53	113	3	4×10^{-5}	4×10^{-5}	0	0
YSC_O6	6×10^{-4}	10^{-4}	2×10^{-6}	9	60	116	3	3×10^{-5}	3×10^{-5}	5×10^{-6}	0
YSC_O7	0.002	2×10^{-4}	5×10^{-6}	9	51	128	3	3×10^{-5}	3×10^{-5}	5×10^{-6}	0

Notes. Column 1: name of the model; column 2 (f_{ng}): fraction of n th-generation mergers with respect to all BBH mergers; column 3 (f_{PI}): fraction of BBH mergers with at least one component in the PI mass gap with respect to all BBH mergers; column 4 (f_{IMBH}): fraction of BBH mergers with at least one IMBH component with respect to all BBH mergers; column 5 (Med m_1): median value of the mass of the primary component of a first-generation BBH merger; column 6 (Med $m_{1,\text{ng}}$): median value of the mass of the primary component of a n th-generation BBH merger; column 7 (Max $m_{1,\text{ng}}$): maximum mass of the primary component of a n th-generation BBH merger; column 8 (N_g): maximum number of generations; column 9 ($f(e > 0.1)$): fraction of BBHs with orbital eccentricity > 0.1 in the LIGO–Virgo band (i.e. when $f_{\text{GW}} = 10$ Hz); column 10 ($f(e > 0.5)$): fraction of BBHs with orbital eccentricity > 0.5 in the LIGO–Virgo band; columns 11 and 12 (f_{GW190521}): fraction of BBHs that match the mass and spin of GW190521, inside the 90 per cent credible interval, when considering Abbott et al. (2020d) and Nitz & Capano (2021), respectively.

to lower values for YSCs ($t_{\text{dyn}} \sim 3\text{--}20$ Myr) than for both GCs ($t_{\text{dyn}} \sim 20\text{--}200$ Myr) and NSCs (peaking at $t_{\text{dyn}} \sim 20\text{--}200$ Myr, but with a considerable fraction of systems with $t_{\text{dyn}} > 1$ Gyr). Indeed, dynamical friction time-scales, three-body time-scales and exchange time-scales are usually shorter in YSCs, which have lower velocity dispersion than both GCs and YSCs, but relatively high central density and large binary fractions (Portegies Zwart et al. 2010; Neumayer et al. 2020).

6.3 Original binaries in NSCs, GCs and YSCs

Figs 4–6 show the same distributions as Fig. 1, but for original binaries in NSCs, GCs and YSCs, respectively (NSC_O1, GC_O1 and YSC_O1). The main differences with respect to dynamical binaries concern the distribution of first-generation masses and eccentricities and the relevant time-scales.

The masses of first-generation original BBHs are skewed to lower values than those of first-generation dynamical BBHs because

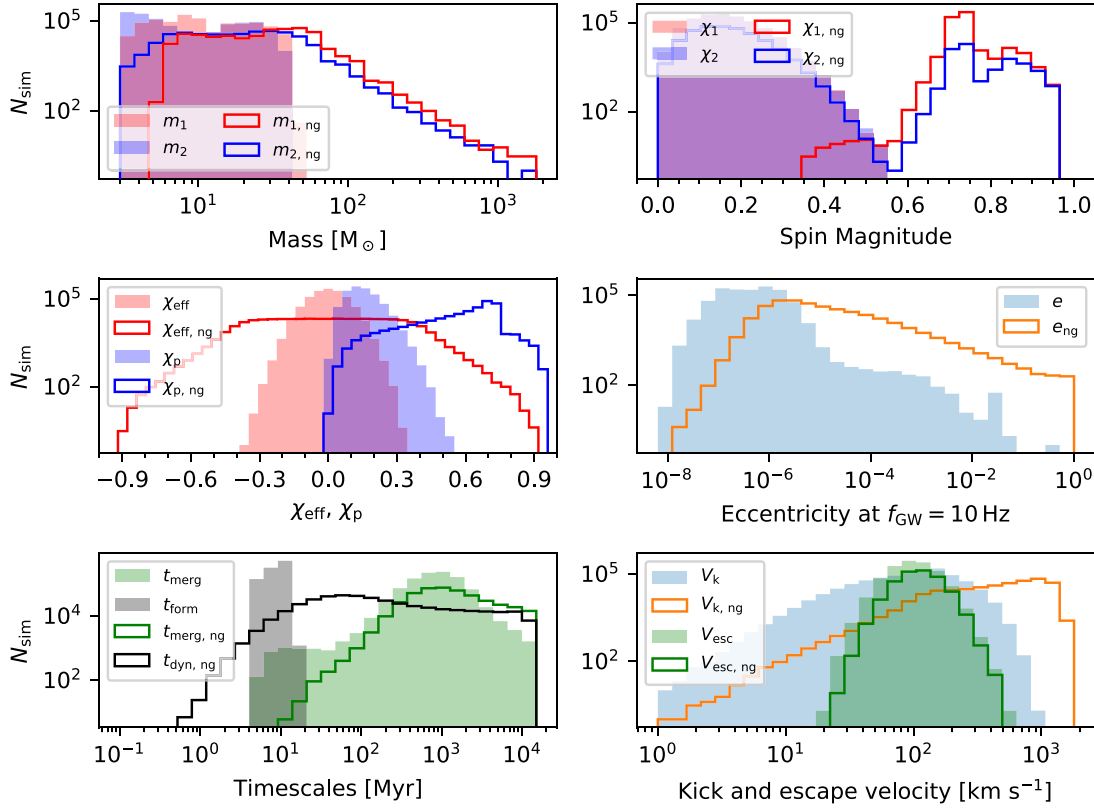


Figure 4. Same as Fig. 1, but for original binaries in NSCs (model NSC.O1). The only difference is the meaning of the filled grey histogram in the lower left-hand panel, which here shows the formation time-scale of the original first-generation BBH (t_{form}), i.e. the time elapsed between the formation of the binary star and the formation of the second BH.

supernova kicks are not as efficient in ejecting binary systems from the parent star cluster and because the maximum mass for the components of a BBH merger is only $\sim 45 M_{\odot}$ in original binaries. This implies that the bulk of n th-generation mergers descending from original binaries is also shifted to lower values with respect to dynamical binaries: $\sim 20\text{--}70 M_{\odot}$ instead of $\sim 30\text{--}100 M_{\odot}$, at $Z = 0.002$. As a consequence, the maximum masses of n th-generation mergers are also shifted to lower values. Even in the case of original binaries, the fraction of n th-generation to first-generation mergers is considerably higher in NSCs than GCs and YSCs.

Even if three-body encounters tend to increase the eccentricity of binary systems, the eccentricities of first-generation original mergers are squeezed to lower values, with almost no systems with eccentricity > 0.1 in the LIGO–Virgo band. n th-generation mergers are the only ones to populate this region. Table 2 shows that this is true not only for the three fiducial models of original binaries (NSC.O1, GC.O1 and YSC.O1), but also for all the other models with one exception: the high-metallicity case. In the models NSC.O3, GC.O3 and YSC.O3 (original binaries with progenitor metallicity $Z = 0.02$) the percentage of mergers with eccentricity $e > 0.1$ is $\approx 1\text{--}2$ per cent. This is not an effect of dynamical encounters, but a consequence of supernova kicks. Most of the highly eccentric systems at solar metallicity are first-generation mergers, which form with high eccentricity because of the supernova kick they receive at birth, right after a common-envelope phase (Giacobbo et al. 2018).

While spin distributions are the same in original and dynamical binaries by construction, the relevant time-scales are remarkably different because the formation time of an original BBH is always between $t_{\text{form}} \approx 3$ and ≈ 20 Myr, corresponding to the formation

time of the second BH. In contrast, the time t_{dyn} for the dynamical assembly of a first-generation BBH varies wildly depending on the properties of both the primary BH and the host star cluster: it could be as short as ~ 3 Myr or as long as $\sim t_{\text{Hubble}}$.

6.4 Impact of metallicity on masses

The metallicity of the progenitors leaves a strong imprint on the mass spectrum of first-generation and, consequently, n th-generation mergers, for both original and dynamical binaries. Fig. 7 shows the primary and secondary masses of dynamical BBHs. The peak of the n th-generation BHs tends to cluster around the maximum mass of first-generation mergers. At solar metallicity, this maximum mass is $\approx 30 M_{\odot}$, while it rises up to $\approx 70 M_{\odot}$ for dynamical binaries at low metallicity.

Table 2 shows the median value of primary BHs’ mass in first- and n th-generation mergers for all the considered models, together with the maximum mass. In NSCs, the median value of primary BH mass in first-generation dynamical binaries is $\approx 20 M_{\odot}$ at low metallicity ($Z = 0.002, 0.0002$) and $\approx 8 M_{\odot}$ at solar metallicity, while the median value in n th-generation mergers is ≈ 35 (≈ 15) M_{\odot} at low (solar) metallicity.

In GCs and YSCs, the median values are considerably larger than in NSCs, for both first-generation and n th-generation dynamical BHs because (as we mentioned before) the lightest single BHs are easily ejected by supernova kicks and cannot pair up dynamically. Hence, in GCs, the median mass of first-generation primary BHs is ≈ 30 (≈ 17) M_{\odot} at low (solar) metallicity, while the median mass of n th-generation primary BHs is ≈ 50 (≈ 30) M_{\odot} at low (solar) metallicity.

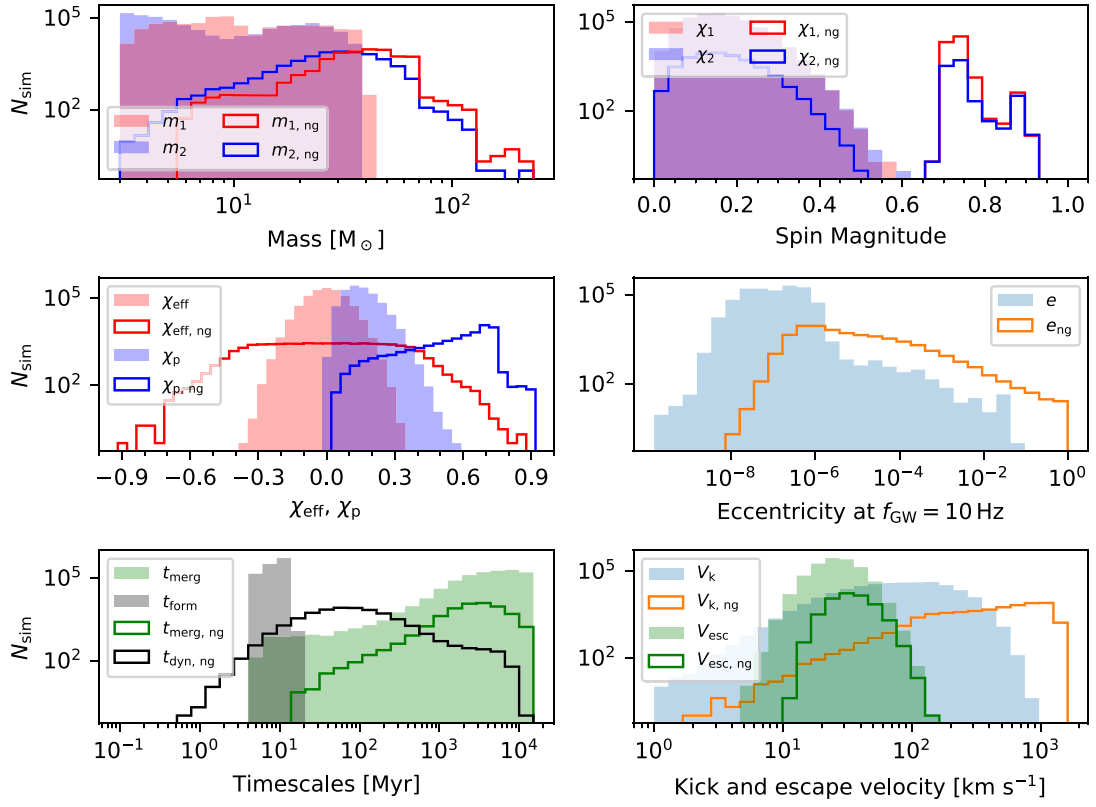


Figure 5. Same as Fig. 4, but for original binaries in GCs. Model GC.O1.

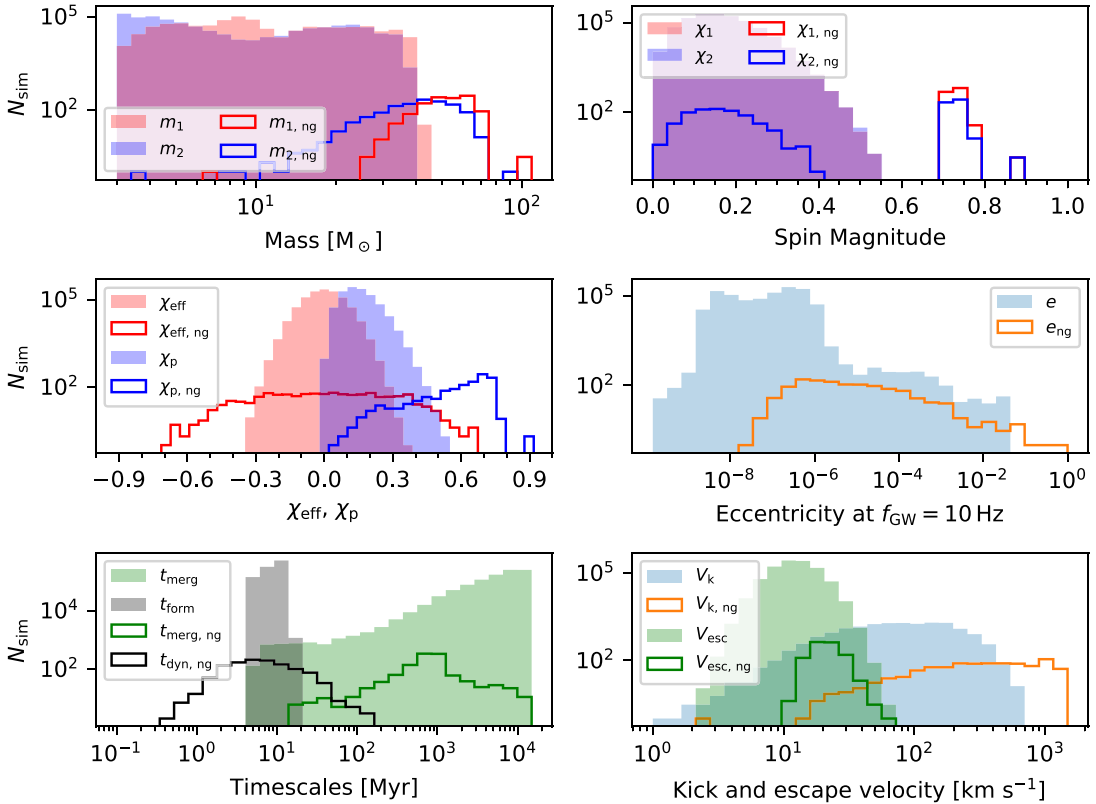


Figure 6. Same as Fig. 4, but for original binaries in YSCs. Model YSC.O1.

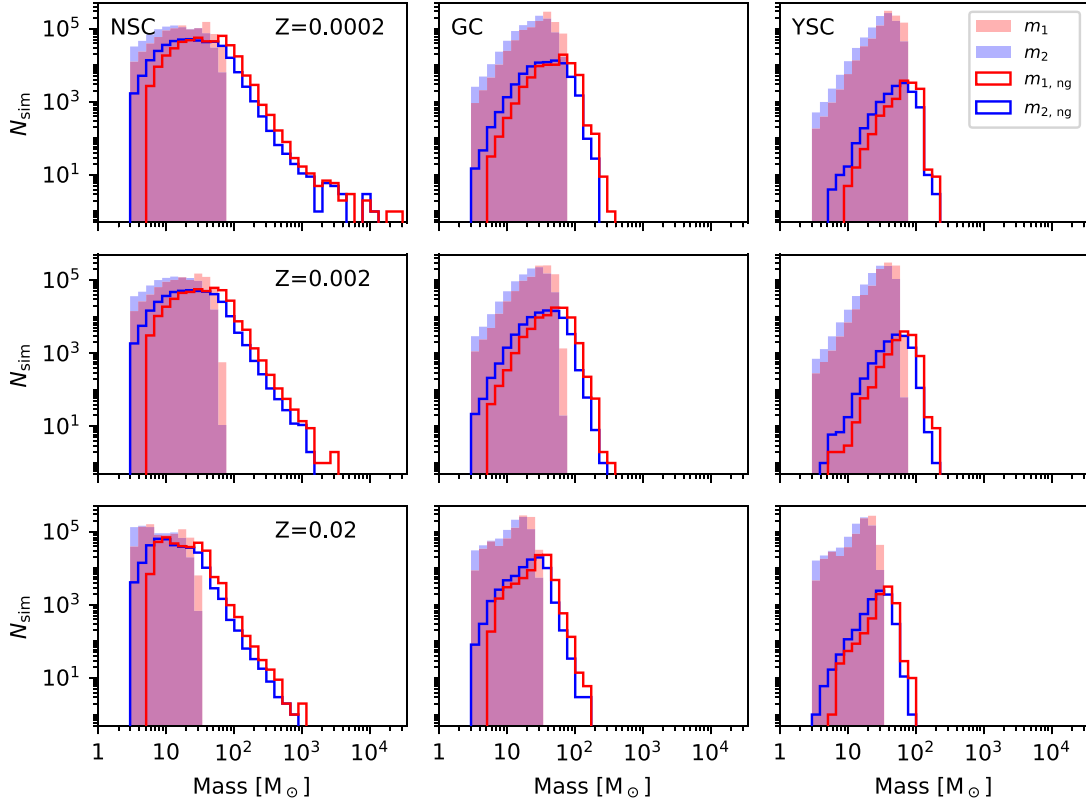


Figure 7. Masses of the BBH mergers for different stellar metallicities and star clusters. From the top to bottom: $Z = 0.0002$, 0.002 and 0.02 . Left-hand panels: NSCs (from the top to bottom: models NSC.D2, NSC.D1 and NSC.D3); middle panels: GCs (models GC.D2, GC.D1 and GC.D3); right-hand panels: YSCs (models YSC.D2, YSC.D1 and YSC.D3). In each panel, the filled red (blue) histogram shows the primary (secondary) mass of first-generation mergers, while the unfilled red (blue) histogram shows the primary (secondary) mass of n th-generation mergers. The y-axis shows the number of simulated BBH mergers.

In YSCs, the median mass of first-generation primary BHs is ≈ 40 (≈ 19) M_{\odot} at low (solar) metallicity, while the median mass of n th-generation primary BHs is ≈ 70 (≈ 40) M_{\odot} at low (solar) metallicity.

We can draw similar conclusions for original binaries, just shifted to lower mass values. For the sake of brevity, we do not show an additional figure for original binaries, but Table 2 clearly shows that the median masses of primary BHs are lower in original binaries. For example, in NSCs, the median mass of primary BHs in first-generation original binaries is 9–10 M_{\odot} at low metallicity and 6 M_{\odot} at solar metallicity. The same quantity for primary BHs of n th-generation binaries is 24–32 M_{\odot} at low metallicity and only 9 M_{\odot} at solar metallicity.

6.5 Impact of spin distribution

The actual distribution of BH spin magnitudes is highly uncertain from both theory (e.g. Bavera et al. 2020; Belczynski et al. 2020) and observations (e.g. Miller & Miller 2015; Abbott et al. 2020b). For this reason, we explore a wide range of values for σ_{χ} . Fig. 8 shows the impact of different spin distributions on the mass of BBHs for dynamical binaries in GCs. We do not show NSCs, YSCs and original binaries because the effect is similar to the one shown in Fig. 8. Different spin magnitudes do not significantly impact the shape of the mass function, the maximum mass and the position of the peak, but they have a strong effect on the number of n th-generation mergers.

This effect is particularly important for YSCs and GCs, which have a lower escape velocity than NSCs. As shown by Fig. 9 and

by Table 2, the fraction of n th-generation mergers f_{ng} over all BBH mergers is only ≈ 0.02 of the total mergers for $\sigma_{\chi} = 0.3$ and for dynamical binaries in GCs, while it rises to ≈ 0.075 for $\sigma_{\chi} = 0.01$. This happens because larger spins are associated with larger relativistic kicks than smaller spin magnitudes, for a given mass ratio and inclination of the spins.

Fig. 8 also shows that the double horned shape of the distribution of χ_p disappears for the large spin case ($\sigma_{\chi} = 0.3$), while it is a strong feature of both the low- and intermediate-spin cases.

6.6 Impact of star cluster mass

Escape velocity is possibly the key quantity to drive the number and properties of n th-generation mergers. Most of the differences between YSCs, GCs and NSCs spring from the different v_{esc} , with a larger escape velocity leading to more n th-generation mergers, and to a higher maximum mass. The parameter that mainly affects the escape velocity is star cluster mass ($v_{esc} \propto M_{tot}^{1/3}$, equation 22).

Fig. 10 shows the distribution of primary masses of n th-generation BBH mergers in NSCs when changing the standard deviation of the total star cluster mass distribution. The good news is that the changes do not affect the position of the peak, which corresponds to masses $m_{1,ng} = 30$ – $80 M_{\odot}$ for both dynamical and original BBHs. On the other hand, a larger standard deviation leads to higher possible maximum masses, associated with the most massive clusters. In the case NSC.D7 ($\sigma_M = 0.6$), the maximum BH mass is $\approx 4.4 \times 10^4 M_{\odot}$, while it is only $\approx 1500 M_{\odot}$ in NSC.D6 ($\sigma_M = 0.2$). Such massive

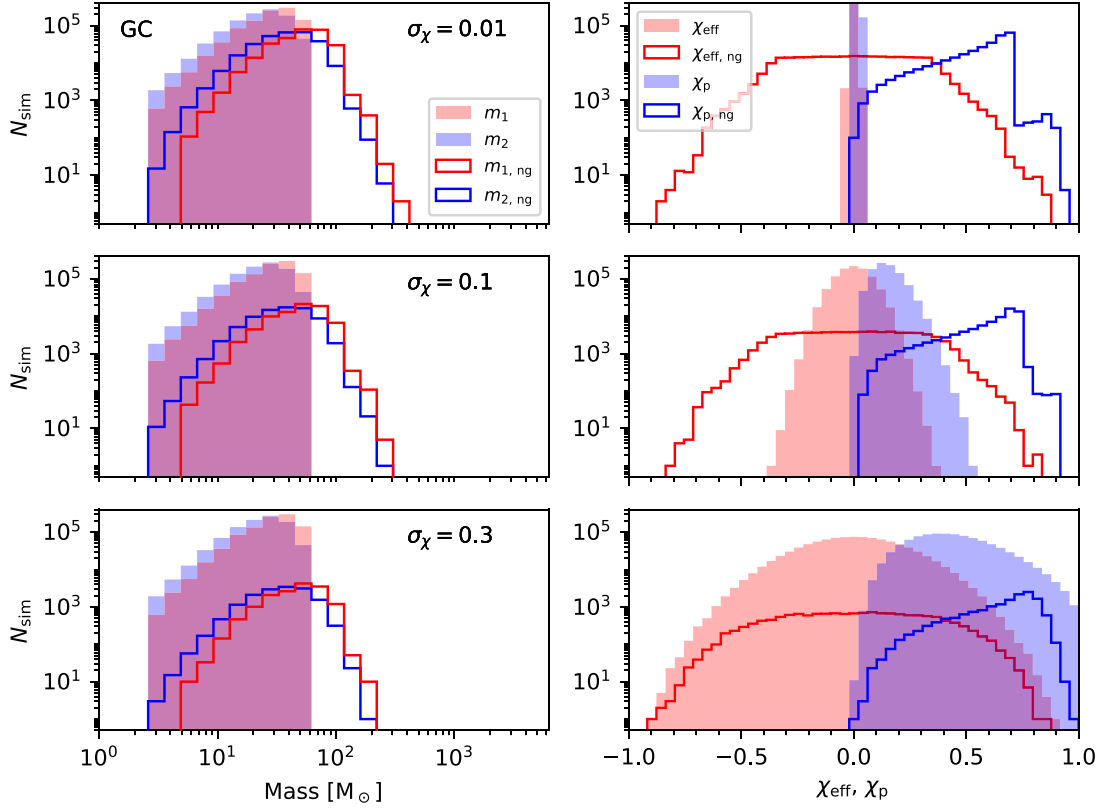


Figure 8. Masses (left-hand panels) and spins (right-hand panels) of the BBH mergers for different initial spin distributions. The figure shows the case of GCs, but we draw similar conclusions for NSCs and YSCs (not shown for brevity). From the top to bottom: first-generation spins drawn from a Maxwellian distribution with one-dimensional root mean square $\sigma_\chi = 0.01$ (upper panels, model GC_D4), 0.1 (central panels, fiducial model GC_D1) and 0.3 (lower panels, model GC_D5). Left-hand panels: The filled red (blue) histogram shows the primary (secondary) mass of first-generation mergers, while the unfilled red (blue) histogram shows the primary (secondary) mass of n th-generation mergers. Right-hand panels: The filled red (blue) histogram shows the effective spin (precessing spin) of first-generation mergers, while the unfilled red (blue) histogram shows the effective spin (precessing spin) of n th-generation mergers. In all the panels, the y-axis shows the number of simulated BBH mergers.

n th-generation BBHs are extremely rare anyway (~ 1 every 10^6 BBH mergers).

Table 2 shows not only the maximum primary BH mass, but also the total number of generations per each model. The effect of varying σ_M on the number of generations N_g is apparent, especially for NSCs: $N_g = 17, 10$ and 8 in NSC_D7 ($\sigma_M = 0.6$), NSC_D1 ($\sigma_M = 0.4$) and NSC_D6 ($\sigma_M = 0.2$), respectively.

6.7 Efficiency of hierarchical mergers

There is a remarkable difference between NSCs and the other types of star clusters, if we look at the efficiency of hierarchical mergers. Here, for efficiency we mean both (i) the fraction of n th-generation mergers with respect to all BBH mergers (f_{ng}) and (ii) the maximum number of generations (N_g) achieved in a given model. Both f_{ng} and N_g are listed in Table 2. Fig. 9 shows the behaviour of f_{ng} across different models.

In NSCs, f_{ng} is almost always $\gtrsim 0.3$, with the exception of the models NSC_O3 (original binaries with solar metallicity), NSC_D5 and NSC_O5 (with $\sigma_\chi = 0.3$). In particular, f_{ng} is a factor of ~ 2 lower for the two high-spin cases. The maximum number of generations is always $N_g \geq 8$. Overall, NSCs are very efficient in producing hierarchical mergers because of their high escape velocity, with just a mild dependence on the other considered parameters, especially the spin magnitudes.

In GCs, f_{ng} changes more wildly, from ~ 0.01 to ~ 0.2 . Most GC models with dynamical (original) binaries have $f_{ng} \approx 0.07$ – 0.08 (≈ 0.04 – 0.06). Models with low and high spins are both outliers: the two low-spin models GC_D4 and GC_O4 have $f_{ng} \approx 0.23$ and ≈ 0.17 , respectively, while the two high-spin cases GC_D5 and GC_O5 have $f_{ng} \approx 0.02$ and ≈ 0.01 . The maximum number of generations ranges from 4 to 6 in all the considered models. Overall, the lower escape velocity of GCs makes the spin magnitude parameter a crucial one to decide the efficiency of hierarchical mergers in GCs.

Finally, YSCs have the lowest efficiency of hierarchical mergers, as expected because of both the lower escape velocity and the shorter lifetime (1 Gyr). In this case, we also see a conspicuous difference between dynamical and original binaries. Most YSC models with dynamical (original) binaries have $f_{ng} \sim 0.01$ ($f_{ng} \sim 10^{-3}$), with a difference of about one order of magnitude between dynamical and original binaries. This is a consequence of the much lower first-generation masses of original binaries with respect to dynamical binaries (Table 2), which makes it even more difficult for the n th-generation systems to merge within a Hubble time, in addition to the short lifetime and low escape velocity of YSCs. Similar to GCs, the spin distribution plays a major role to further suppress or enhance the fraction of n th-generation mergers in YSCs: $f_{ng} \approx 0.096$ and 0.002 according to models YSC_D4 ($\sigma_\chi = 0.01$) and YSC_D5 ($\sigma_\chi = 0.3$). The maximum number of generations is always between 3 and 4.

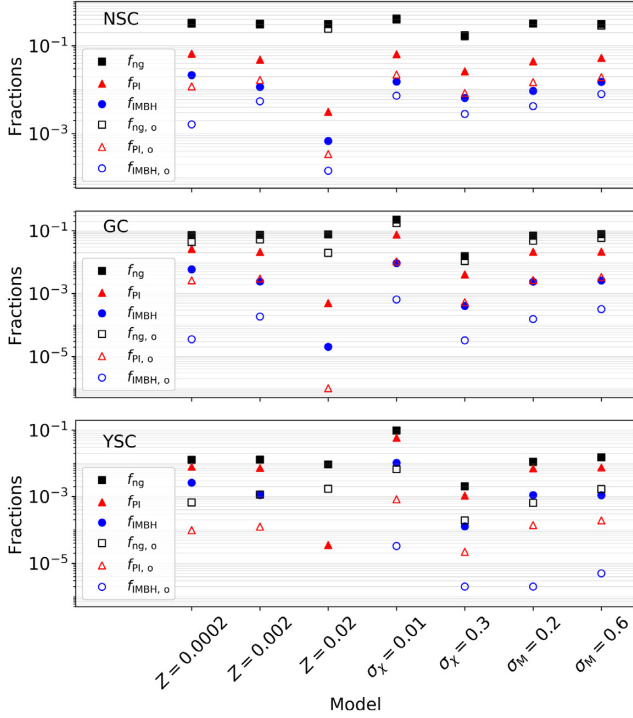


Figure 9. Black squares: fraction f_{ng} of n th-generation BBH mergers over the total number of BBH mergers (including both first- and n th-generation mergers). Red triangles: fraction f_{PI} of BBH mergers with a primary mass in the PI gap (65–120 M_{\odot}) with respect to the total number of BBH mergers. Blue circles: fraction f_{IMBH} of BBH mergers with a primary mass in the intermediate-mass BH regime (100–10⁵ M_{\odot}) with respect to the total number of BBH mergers. Filled (open) symbols refer to dynamical (original) binaries. The models labelled as $Z = 0.0002$ are NSC_D2, GC_D2, YSC_D2, NSC_O2, GC_O2 and YSC_O2, i.e. all the cases with metallicity $Z = 0.0002$. Those labelled as $Z = 0.002$ are NSC_D1, GC_D1, YSC_D1, NSC_O1, GC_O1 and YSC_O1, i.e. all the fiducial cases with $Z = 0.002$, $\sigma_{\chi} = 0.1$ and $\sigma_M = 0.4$. Those labelled as $Z = 0.02$ are NSC_D3, GC_D3, YSC_D3, NSC_O3, GC_O3 and YSC_O3, i.e. all the cases with $Z = 0.02$. Those labelled as $\sigma_{\chi} = 0.01$ ($\sigma_{\chi} = 0.3$) are NSC_D4, GC_D4, YSC_D4, NSC_O4, GC_O4 and YSC_O4 (NSC_D5, GC_D5, YSC_D5, NSC_O5, GC_O5 and YSC_O5), i.e. all the cases with $\sigma_{\chi} = 0.01$ ($\sigma_{\chi} = 0.3$). Those labelled as $\sigma_M = 0.2$ ($\sigma_M = 0.6$) are NSC_D6, GC_D6, YSC_D6, NSC_O6, GC_O6 and YSC_O6 (NSC_D7, GC_D7, YSC_D7, NSC_O7, GC_O7 and YSC_O7), i.e. all the cases with $\sigma_M = 0.2$ ($\sigma_M = 0.6$).

To summarize, the efficiency of hierarchical mergers is always larger in NSCs than either GCs or YSCs, mostly as a result of the escape velocity. Large (small) spins tend to suppress (enhance) the efficiency of hierarchical mergers, but their impact is much larger for both GCs and YSCs than for NSCs. Original binaries are less efficient in leading to the hierarchical growth with respect to the more massive dynamical binaries. Overall, NSCs are less sensitive to the main parameters (including spin magnitudes) with respect to both GCs and YSCs.

Even if we can reach up to 17 generations in the most lucky case (NSC_D7), the fraction of BBH mergers in each generation with respect to the total number of BBH mergers decreases very fast. The lower panel of Fig. 11 shows that the fraction of mergers in the last generation is lower than 10⁻⁴. The second generation is always at least one order of magnitude more populated than the next one.

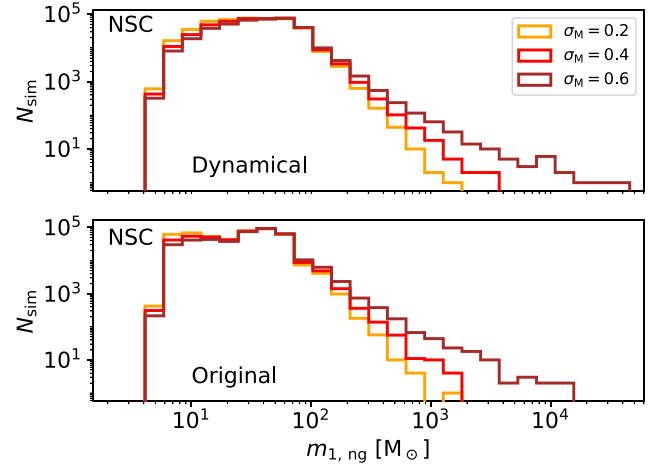


Figure 10. Primary mass distribution for n th-generation BBHs in NSCs. Upper panel: dynamical BBHs; lower panel: original BBHs. Orange line: models with $\sigma_M = 0.2$ (NSC_D6 and NSC_O6 in the upper and lower panels, respectively); light red line: models with $\sigma_M = 0.4$ (NSC_D1 and NSC_O1 in the upper and lower panels, respectively); dark red line: models with $\sigma_M = 0.6$ (NSC_D7 and NSC_O7 in the upper and lower panels, respectively).

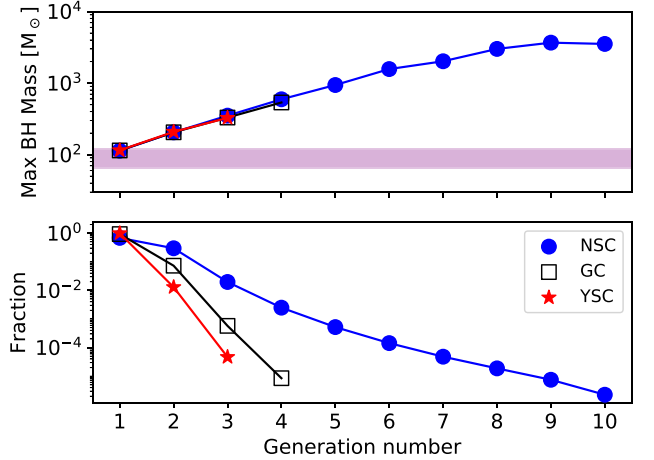


Figure 11. Upper panel: maximum merger remnant mass in each generation as a function of the generation number (where 1 means first generation). Lower panel: Fraction of mergers belonging to a given generation with respect to all BBH mergers in the considered model as a function of the generation number. Red stars: YSCs from the fiducial model for dynamical BBHs (YSC_D1). Open black squares: GCs from the fiducial model for dynamical BBHs (GC_D1). Filled blue circles: NSCs from the fiducial model for dynamical BBHs (NSC_D1).

6.8 BHs in the PI gap and intermediate-mass BHs

Hierarchical mergers are one of the most likely scenarios to form BHs in the PI mass gap and even intermediate-mass BHs (IMBHs). Indeed, we have probably already witnessed the formation of an IMBH via the merger of two smaller BHs (GW190521; Abbott et al. 2020d,g). Our synthetic models show that the population of BHs in the mass gap and IMBHs is extremely sensitive to the metallicity of the progenitor stars and to the properties of the host star cluster (mass and density).

Fig. 9 shows the fraction of BBH mergers that have at least the primary mass in the mass gap (f_{PI}) with respect to all BBH mergers of first- and n th-generation. The values of f_{PI} are also listed in Table 2.

We calculated f_{PI} by assuming the mass gap to be between 65 and $120 M_{\odot}$, given the uncertainties on its boundaries (e.g. Farmer et al. 2019, 2020; Mapelli et al. 2020b; Renzo et al. 2020a; Tanikawa et al. 2020; van Son et al. 2020; Costa et al. 2021; Farrell et al. 2021).

While the fraction of n th-generation mergers f_{ng} is almost insensitive to stellar metallicity, f_{PI} varies wildly depending on this parameter. For example, if we consider dynamical binaries in NSCs, f_{PI} decreases from ~ 0.05 – 0.07 to ~ 0.003 if we go from the metal-poor ($Z = 0.0002, 0.002$) to the metal-rich ($Z = 0.02$) cases. The reason for this feature is that the mass of first-generation BHs is crucial to determine how many second-generation BHs form with mass in the PI gap, and the mass of first-generation BHs strongly depends on progenitors' metallicity in our models.

For the same reason, f_{PI} is considerably lower for original binaries than for dynamical binaries. This happens because the mass of first-generation original mergers is lower than the mass of first-generation dynamical binaries. For example, $f_{\text{PI}} \approx 0.048$ and 0.017 in NSC.D1 and NSC.O1, respectively.

GCs and YSCs are generally associated with lower values of f_{PI} with respect to NSCs. For example, in the fiducial dynamical case, $f_{\text{PI}} \approx 0.048, 0.021$ and 0.007 in NSCs, GCs and YSCs, respectively. There is one exception, though: If the spin magnitudes are very low, f_{PI} is comparable in all types of star clusters: $f_{\text{PI}} \approx 0.064, 0.075$ and 0.059 in NSC.D4, GC.D4 and YSC.D4, respectively. This happens for the same reason as for f_{ng} : when the spins are very low (as our $\sigma_{\chi} = 0.01$ case), the retention fraction of second-generation BHs dramatically rises in lower mass clusters and becomes comparable to NSCs.

We can draw similar statements for the fraction (f_{IMBH}) of merging binaries that include at least one IMBH over all BBH mergers. We consider IMBHs all the simulated BHs with mass $\geq 100 M_{\odot}$, according to an historical definition (Miller & Colbert 2004). Fig. 9 and Table 2 show the values of f_{IMBH} for all the considered cases. f_{IMBH} can be as high as ≈ 0.02 in the case of dynamical binaries in NSCs and as low as 0 in the case of original binaries in YSCs. It is higher (lower) in metal-poor (metal-rich) star clusters and when we consider dynamical (original) binaries. The value of f_{IMBH} is particularly high in GCs and YSCs when the low-spin case is considered. For example, f_{IMBH} rises from ≈ 0.001 in the model YSC.D1 to ≈ 0.01 in YSC.D4.

The upper panel of Fig. 11 shows the maximum mass of the merger remnant in each generation for the fiducial case (NSC.D1, GC.D1 and YSC.D1). The maximum remnant mass is already in the IMBH regime after the first generation. There is not much difference between NSCs, GCs and YSCs if we consider the same generation number. NSCs end building up larger BHs only because they can witness a larger number of generations with respect to both YSCs and GCs. The maximum remnant mass in the most extreme generations ($n \sim 3$ for YSCs, ~ 4 for GCs and ~ 10 for NSCs) is close to $\sim 10^{-3} M_{\text{tot}}$ (where M_{tot} is the total cluster mass), analogous to some previous numerical results (e.g. Portegies Zwart & McMillan 2002; Giersz et al. 2015; Di Carlo et al. 2019; Kroupa et al. 2020) and reminiscent of the observational relationship between the mass of an NSC and that of its central BH in the considered mass range (e.g. Graham & Spitler 2009; Neumayer et al. 2020). Finally, Fig. 12 shows the time evolution of the remnant mass in model NSC.D1 for 15 randomly selected systems. The duration of the hierarchical growth ranges from ≈ 100 Myr to several Gyr in NSCs.

6.9 GW190521: inside the gap or intermediate-mass ratio inspiral?

We explore the possibility that a system like GW190521 forms from our hierarchical models. Previous studies have already investigated

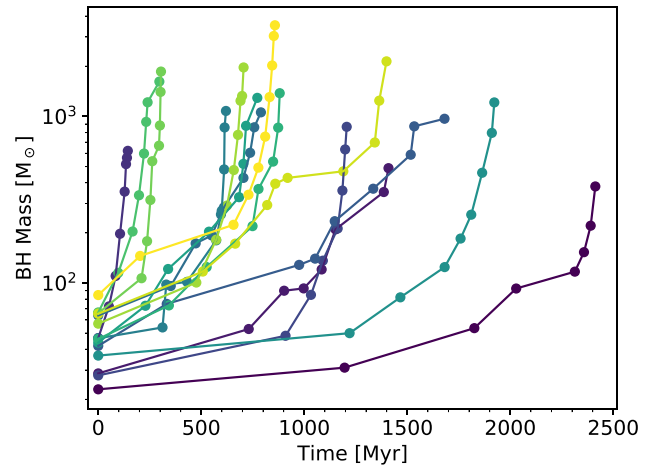


Figure 12. Time evolution of the BH remnant mass for 15 randomly selected hierarchical mergers reaching at least the eighth generation in model NSC.D1. Each circle marks a merger. We set to zero the time of the first-generation merger.

the formation of GW190521 via hierarchical mergers (e.g. Abbott et al. 2020g; Fishbach & Holz 2020; Fragione, Loeb & Rasio 2020a; Fragione et al. 2020b; Gayathri et al. 2020; Palmese & Conselice 2020; Romero-Shaw et al. 2020; Safarzadeh & Haiman 2020; Samsing & Hotokezaka 2020; De Luca et al. 2021b; Liu & Lai 2021; Rice & Zhang 2021; Rizzuto et al. 2021). Also, Kimball et al. (2020a) find that GW190521 is favoured to contain two second-generation BHs with odds > 700 . Our results confirm that this scenario is able to match both the masses and the spins of GW190521 (Table 2). Recently, Nitz & Capano (2021) reanalysed the data of the LIGO–Virgo collaboration (LVC) with a new waveform allowing for more extreme mass ratios. They find that GW190521 is consistent with an intermediate-mass ratio inspiral with primary mass $m_1 = 168^{+15}_{-61} M_{\odot}$ and secondary mass $m_2 = 16^{+33}_{-3} M_{\odot}$ (within 90 per cent credible interval, according to a uniform in mass-ratio prior). In this case, the primary mass is not inside the PI mass gap. We have calculated how many of our systems have both masses and spin parameters inside the 90 per cent credible interval inferred by Nitz & Capano (2021) and by Abbott et al. (2020d), respectively. As shown by Table 2 and Fig. 13, our results indicate that the properties of GW190521-like systems inferred from the analysis of Nitz & Capano (2021) are more difficult to match by the hierarchical merger scenario than the properties inferred by Abbott et al. (2020d). For example, in the model NSC.D1, the fraction of GW190521-like systems over all possible BBH mergers is $f_{\text{GW190521}} \approx 0.02$ and $\approx 4 \times 10^{-4}$ if we use the mass and spin parameters from Abbott et al. (2020d) and Nitz & Capano (2021), respectively. Hence, the new estimates from Nitz & Capano (2021) pose GW190521 on the ‘safe side’ with respect to PI theory, but might be even more difficult to explain with an astrophysical model. Our assumption for the mass distribution of secondary BHs (equation 9), motivated by previous star cluster simulations, strongly influences this result.

Finally, Gayathri et al. (2020) and Romero-Shaw et al. (2020) propose that GW190521 is consistent with an eccentric BBH merger. Among all the systems that match the mass and spin of GW190521 in our models, the fraction of those that have eccentricity $e > 0.5$ in the LIGO–Virgo band is $\sim 10^{-3}$ in our fiducial dynamical models. However, our current formalism does not include GW captures (Zevin et al. 2019). Hence, the fraction of systems with extreme eccentricity we estimated should be regarded as a lower limit.

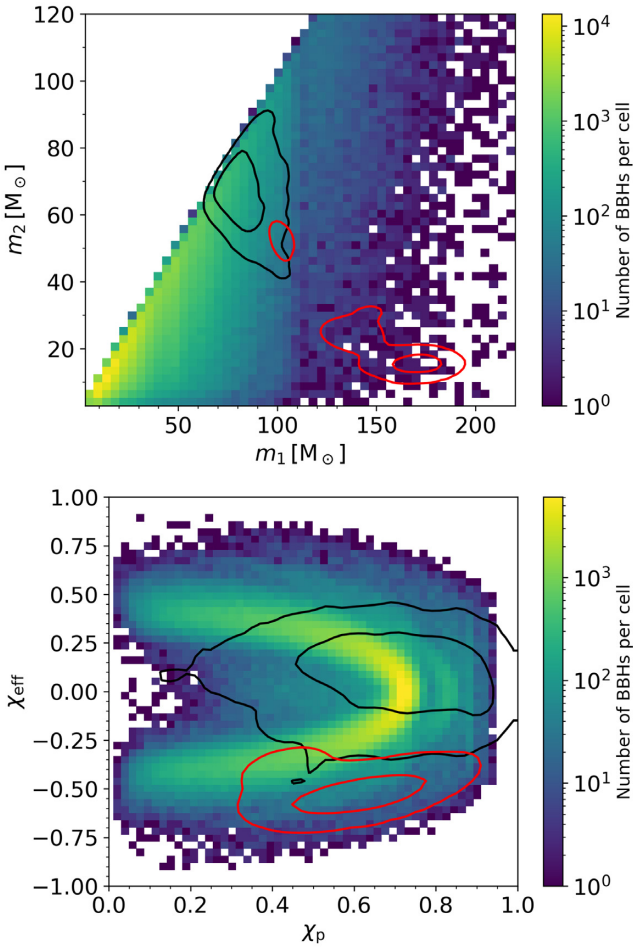


Figure 13. Upper panel: mass of secondary versus primary component of n th-generation BBH mergers in model NSC.D1. Lower panel: effective versus precessing spin of n th-generation BBH mergers in NSC.D1. In both plots, the contours show the 90 and 50 per cent credible intervals for GW190521 according to Abbott et al. (2020d), in black, and Nitz & Capano (2021), in red, respectively.

7 DISCUSSION

We studied the evolution of hierarchical mergers born from both dynamical and original binaries. The latter have been overlooked in previous work. In our treatment, we did not attempt to quantify the relative weight of original versus dynamical binaries. Are dynamical or original binaries more representative of the actual population of BBH mergers in star clusters? A reasonable guess is that YSCs should be dominated by original binaries because they have a binary fraction close to 1 (e.g. Sana et al. 2012). In contrast, NSCs are probably dominated by dynamical binaries because most original binaries are too soft and get ionized, while GCs should stay in between. In a follow-up study, we will try to constrain the relative fraction of original versus dynamical binaries in different star clusters. Overall, the main differences between a star cluster dominated by original binaries and one dominated by dynamical binaries are (i) the mass distribution of first-generation BBHs (more squeezed towards lower values for original binaries), (ii) the global distribution of eccentricities in the LIGO–Virgo band (original binaries inherit lower eccentricities from binary star evolution) and (iii) the efficiency of hierarchical mergers and formation of BBHs in the PI gap or IMBHs.

The formalism presented here might lead to an overestimation of the differences between original and dynamical binaries. In fact, even original binaries can undergo dynamical exchanges before the two original members of the binary merge. Dynamical exchanges are currently not implemented in our model and tend to lead to the formation of more and more massive binary systems, which are more energetically stable (Hills & Fullerton 1980). Hence, exchanges might reduce the differences between the mass function of original and dynamical binaries.

Moreover, we have not included stellar and binary evolution. This leads us to neglect star–star collisions and runaway mergers, which are triggered by dynamical encounters and can be an additional formation channel of BHs in the PI mass gap and IMBHs, especially in metal-poor YSCs (Di Carlo et al. 2019, 2020a,b; Kremer et al. 2020; Renzo et al. 2020b). Given their short dynamical friction and core collapse time-scales, YSCs are particularly efficient in forming massive BHs via runaway collisions (e.g. Portegies Zwart et al. 2004; Giersz et al. 2015; Mapelli 2016). Hence, including stellar collisions might bridge the gap between YSCs and more massive clusters, leading to comparable values of f_{PI} and f_{IMBH} .

We have assumed that the properties of a star cluster do not evolve during its life. On the one hand, star clusters lose mass by stellar evolution and dynamical ejection and expand by two-body relaxation. This leads to lower star cluster mass and density, possibly quenching the formation of hierarchical mergers (e.g. Antonini & Gieles 2020a,c). On the other hand, by assuming no evolution with time, we do not account for core collapse episodes and gravothermal oscillations, which lead to a dramatic temporary increase of the central density, possibly boosting BBH formation and hierarchical mergers (e.g. Breen & Heggie 2013). NSCs might even acquire mass during their life by fresh star formation (e.g. Mapelli et al. 2012) and by accreting GCs (e.g. Capuzzo-Dolcetta & Miocchi 2008; Antonini et al. 2012). These processes might lead to a higher efficiency of hierarchical mergers in NSCs. The overall effect of including star cluster evolution in our model is thus quite difficult to predict and might be significantly different for YSCs, GCs and NSCs. We will add a formalism for star cluster evolution in a follow-up study.

Furthermore, we assumed that each BBH, after formation, remains inside the cluster core until it merges or it is ejected from the cluster. This might overestimate the effect of dynamical hardening because the binary may wander around the cluster as an effect of three-body encounters and Brownian motion (e.g. Arca Sedda 2020).

Several previous studies have investigated hierarchical mergers either with simulations or semianalytic models. We briefly compare our main results against some relevant previous work. The possibility of growing large IMBHs (up to $\sim 4 \times 10^4 M_\odot$ in our simulations) when particularly massive ($> 10^7 M_\odot$) NSCs are considered is in good agreement with previous semianalytic models (e.g. Antonini et al. 2019; Fragione & Silk 2020; Mapelli et al. 2020a). Similar to Baibhav et al. (2020), we recover the prediction of a spin gap between first-generation and n th-generation mergers, when we consider relatively low values of the spin parameter ($\sigma_\chi = 0.01, 0.1$) for first-generation BHs.

The strong impact of the initial spin magnitude distribution on both f_{ng} and f_{PI} confirms a previous result by Rodriguez et al. (2019), based on dynamical simulations. They find that ~ 10 per cent (~ 1 per cent) of the BBH mergers in their simulated GCs have mass in the PI gap when a constant value of $\chi = 0$ ($\chi = 0.5$) is assumed. For comparison, in our models GC.D4 ($\sigma_\chi = 0.01$) and GC.D5 ($\sigma_\chi = 0.3$), we obtain $f_{\text{PI}} \approx 0.075$ and 0.004 , respectively. These numbers and the results of Rodriguez et al. (2019) are in fair agreement, if we take into account

the differences among the two methods (e.g. a constant value versus a Maxwellian distribution for the spin magnitudes). With respect to both Rodriguez et al. (2019) and Zevin et al. (2019), we find significantly less systems with extreme eccentricity in the LVC band. This happens because we do not include GW captures in our model. In this sense, our eccentricity distribution should be regarded as a lower limit.

Kimball et al. (2020a) study the properties of BBH mergers in GWTC-2 with a phenomenological population model, optimized for GCs (see also Kimball et al. 2020b and Doctor et al. 2020). They conclude that the rate of mergers between a second-generation and a first-generation BH is about one order of magnitude lower than the one of first-generation BBHs. It is almost impossible to make a one-to-one comparison between our results and these models because of the intrinsic differences of the methodology, but the order of magnitude is the same as the values of f_{ng} reported in Table 2 for most NSC and GC models.

In summary, our new tool compares quite well with the results of previous semianalytic models and dynamical simulations. It is particularly flexible, because we can start from different binary catalogues, based on either population synthesis or phenomenological models, and is considerably fast: We can integrate the hierarchical merger of $\approx 10^6$ initial binaries per single core per day. This will allow a future exploration of an even larger parameter space than the one considered here.

8 SUMMARY

We investigated the hierarchical merger scenario with a new fast synthetic tool: FASTCLUSTER evolves a population of BBHs in star clusters, taking into account both hardening by three-body encounters and GW decay. The first-generation BBHs we considered in this work have two possible formation channels: original and dynamical BBHs. The former descend from hard binary stars, while the latter assembly via dynamical friction, three-body encounters and dynamical exchanges. We evolve the first- and n th-generation binaries in three different environments: YSCs, GCs and NSCs. We explore different progenitor metallicities ($Z = 0.0002, 0.002$ and 0.02), spin magnitude distributions ($\sigma_\chi = 0.01, 0.1$ and 0.3) and star cluster mass distributions ($\sigma_M = 0.2, 0.4$ and 0.6).

First-generation dynamical binaries have larger average masses than original binaries because only BHs with mass up to $\sim 45 M_\odot$ can form in hard original binaries, as a consequence of non-conservative mass transfer and common envelope, while dynamical binaries tend to host more massive first-generation BHs (up to $\sim 65 M_\odot$), which harden faster.

The median values of the primary BH mass in dynamical BBH mergers are larger in both YSCs and GCs than in NSCs (see Table 2). This seemingly odd result is a consequence of supernova kicks. BHs ejected by supernova kicks cannot pair up dynamically. In YSCs and GCs, the lighter BHs are ejected by the supernova kick and do not participate to the dynamical assembly. In contrast, NSCs, which have a much higher escape velocity, retain a larger fraction of light BHs.

The bulk of the population of n th-generation BHs has mass comparable with the maximum mass of first-generation BH mergers. Progenitor's metallicity has a strong impact on the typical mass of first- and n th-generation BBHs, both in original and dynamical binaries. For example, in our fiducial case for dynamical binaries in NSCs (NSC.D1), the median mass of the primary BH in first-generation (n th-generation) mergers is $\approx 20 M_\odot$ ($\approx 35 M_\odot$) in metal-poor clusters, while it drops to $\approx 8 M_\odot$ ($\approx 15 M_\odot$) at solar metallicity.

The maximum possible BH mass is much larger in NSCs than in both YSCs and GCs because of the higher escape velocity, which allows to build up a larger number of generations. In our fiducial cases, we form BHs with mass up to a few thousand M_\odot in NSCs and up to a few hundred M_\odot in both GCs and YSCs. NSCs host up to 10 generations in the fiducial case (and up to 17 in the most optimistic case), while GCs and YSCs typically witness up to 4–5 and 3–4 generations, respectively.

Original binaries tend to have lower eccentricity than dynamical binaries because of the impact of binary evolution processes. n th-generation mergers are all the result of dynamical assembly and tend to compensate this initial difference between first-generation dynamical and original binaries. Overall, large eccentricities in the LIGO–Virgo band are extremely rare. For example, the fraction of mergers with eccentricity $e > 0.1$ ($e > 0.5$) in the LIGO–Virgo band is ≈ 0.002 (10^{-4}) for the dynamical binaries and 6×10^{-4} (10^{-4}) for the original binaries in our fiducial case for NSCs, when we consider all the generations together.

Spin magnitudes affect mostly the number of n th-generation mergers with respect to first-generation. This effect is particularly strong in YSCs and GCs. NSCs are less sensitive to spins because of their higher escape velocity. The most relevant feature in the spin distribution of the global population (including both first- and n th-generation mergers) is the double horned distribution of the precessing spin χ_p . This shape appears in the models where we assume that first-generation spin magnitudes are small. For example, in our fiducial cases, first-generation mergers peak at $\chi_p \sim 0.1$ – 0.2 , while n th-generation mergers peak at $\chi_p \sim 0.7$.

We calculate the fraction f_{ng} of n th-generation mergers over all possible BBH mergers. f_{ng} is of the order of ≈ 0.3 (≈ 0.3), ≈ 0.07 (≈ 0.05) and ≈ 0.01 (≈ 0.001) for our fiducial model of dynamical (original) binaries in NSCs, GCs and YSCs, respectively. Hence, the n th-generation fraction is maximum for NSCs, where it is also rather insensitive to the considered parameters. In GCs and YSCs, this fraction is highly sensitive to the spin magnitude; for example, in GCs f_{ng} is up to ~ 0.23 if the spin parameter $\sigma_\chi = 0.01$ and down to ~ 0.02 if $\sigma_\chi = 0.3$. This happens because larger spins lead to stronger relativistic kicks, able to eject the merger remnant. NSCs are less sensitive to this difference (f_{ng} changes only by a factor of 2 between the low-spin and the high-spin case) because of their high escape velocity.

Hierarchical mergers efficiently trigger the formation of BBHs with primary mass in the PI mass gap or in the IMBH regime. In our fiducial cases for dynamical binaries (with $Z = 0.002$), the fraction of mergers with primary mass in the PI gap is $f_{\text{PI}} \approx 0.048, 0.021$ and 0.007 for NSCs, GCs and YSCs, respectively. In the same models, the fraction of mergers with primary mass in the IMBH regime is $f_{\text{IMBH}} \approx 0.012, 0.002$ and 0.001 for NSCs, GCs and YSCs, respectively.

Unlike the global fraction of n th-generation mergers, the fraction of BBHs in the PI mass gap and in the IMBH regime is dramatically affected by metallicity (Table 2). For example, f_{PI} drops by a factor of ≈ 40 in GCs, if we go from $Z = 0.002$ to 0.02 . Spins are also important, with lower spins enhancing the fraction of mergers in the mass gap and in the IMBH regime with respect to larger spins.

Finally, we investigated the possibility that GW190521 is the result of a hierarchical merger. A recent re-analysis of the LVC data (Nitz & Capano 2021) indicates that this event might be explained by the merger between an IMBH ($\sim 168 M_\odot$) and an $\sim 16 M_\odot$ companion. We estimate the fraction of simulated mergers that match the mass and spin of GW190521 within the 90 per cent credible interval if we assume the values from Abbott et al. (2020d) and Nitz & Capano (2021), respectively. In all our models, it is much easier to produce

a system matching the parameters derived by Abbott et al. (2020d) with respect to Nitz & Capano (2021). For example, in the model NSC.D1, the fraction of BBH mergers inside the 90 per cent credible interval of GW190521 are ≈ 0.019 and 4×10^{-4} if we take masses and spins from Abbott et al. (2020d) and Nitz & Capano (2021), respectively. The interpretation proposed by Nitz & Capano (2021) does not require a violation of the PI mass gap, but might be even more difficult to explain with current astrophysical models.

ACKNOWLEDGEMENTS

We thank the anonymous referee for their insightful comments, which helped improve this work. We also thank Isobel Romero-Shaw for useful discussions. MM, AB, YB, UNDC, NG, GI and FS acknowledge financial support from the European Research Council for the ERC Consolidator grant DEMOBLACK, under contract no. 770017. MCA and MM acknowledge financial support from the Austrian National Science Foundation through FWF stand-alone grant P31154-N27. NG is supported by Leverhulme Trust Grant No. RPG-2019-350 and Royal Society Grant No. RGS-R2-202004. MAS acknowledges financial support from the Alexander von Humboldt Foundation for the research program ‘The evolution of black holes from stellar to galactic scales’, the Volkswagen Foundation Trilateral Partnership through project No. I/97778 and the Deutsche Forschungsgemeinschaft (DFG) – Project-ID 138713538 – SFB 881.

DATA AVAILABILITY

The data underlying this paper will be shared on reasonable request to the corresponding authors.

REFERENCES

Aasi J. et al., 2015, *Class. Quantum Gravity*, 32, 074001
 Abbott B. P. et al., 2016a, *Phys. Rev. X*, 6, 041015
 Abbott B. P. et al., 2016b, *Phys. Rev. Lett.*, 116, 061102
 Abbott B. P. et al., 2016c, *ApJ*, 818, L22
 Abbott B. P. et al., 2017, *Phys. Rev. Lett.*, 119, 161101
 Abbott B. P. et al., 2019a, *Phys. Rev. X*, 9, 031040
 Abbott B. P. et al., 2019b, *ApJ*, 882, L24
 Abbott R. et al., 2020a, preprint (arXiv:2010.14527)
 Abbott R. et al., 2020b, preprint (arXiv:2010.14533)
 Abbott R. et al., 2020c, *Phys. Rev. D*, 102, 043015
 Abbott R. et al., 2020d, *Phys. Rev. Lett.*, 125, 101102
 Abbott B. P. et al., 2020e, *ApJ*, 892, L3
 Abbott R. et al., 2020f, *ApJ*, 896, L44
 Abbott R. et al., 2020g, *ApJ*, 900, L13
 Acernese F. et al., 2015, *Class. Quantum Gravity*, 32, 024001
 Ali-Haïmoud Y., Kovetz E. D., Kamionkowski M., 2017, *Phys. Rev. D*, 96, 123523
 Anders E., Grevesse N., 1989, *Geochim. Cosmochim. Acta*, 53, 197
 Antonini F., Gieles M., 2020a, *Phys. Rev. D*, 102, 123016
 Antonini F., Gieles M., 2020b, *MNRAS*, 492, 2936
 Antonini F., Gieles M., 2020c, *MNRAS*, 492, 2936
 Antonini F., Rasio F. A., 2016, *ApJ*, 831, 187
 Antonini F., Capuzzo-Dolcetta R., Mastrobuono-Battisti A., Merritt D., 2012, *ApJ*, 750, 111
 Antonini F., Chatterjee S., Rodriguez C. L., Morscher M., Pattabiraman B., Kalogera V., Rasio F. A., 2016, *ApJ*, 816, 65
 Antonini F., Toonen S., Hamers A. S., 2017, *ApJ*, 841, 77
 Antonini F., Gieles M., Gualandris A., 2019, *MNRAS*, 486, 5008
 Arca Sedda M., 2020, *ApJ*, 891, 47
 Arca Sedda M., Benacquista M., 2019, *MNRAS*, 482, 2991

Arca Sedda M., Mapelli M., Spera M., Benacquista M., Giacobbo N., 2020, *ApJ*, 894, 133
 Arca-Sedda M., Capuzzo-Dolcetta R., 2019, *MNRAS*, 483, 152
 Arca-Sedda M., Gualandris A., 2018, *MNRAS*, 477, 4423
 Arca-Sedda M., Li G., Kocsis B., 2018, preprint (arXiv:1805.06458)
 Askar A., Szkudlarek M., Gondek-Rosińska D., Giersz M., Bulik T., 2017, *MNRAS*, 464, L36
 Baibhav V., Gerosa D., Berti E., Wong K. W. K., Helfer T., Mould M., 2020, *Phys. Rev. D*, 102, 043002
 Banerjee S., 2017, *MNRAS*, 467, 524
 Banerjee S., 2018, *MNRAS*, 473, 909
 Banerjee S., 2021, *MNRAS*, 500, 3002
 Banerjee S., Baumgardt H., Kroupa P., 2010, *MNRAS*, 402, 371
 Bartos I., Kocsis B., Haiman Z., Márka S., 2017, *ApJ*, 835, 165
 Bavera S. S. et al., 2020, *A&A*, 635, A97
 Belczynski K. et al., 2016b, *A&A*, 594, A97
 Belczynski K. et al., 2020, *A&A*, 636, A104
 Belczynski K., 2020, *ApJ*, 905, L15
 Belczynski K., Banerjee S., 2020, *A&A*, 640, L20
 Belczynski K., Kalogera V., Bulik T., 2002, *ApJ*, 572, 407
 Belczynski K., Kalogera V., Rasio F. A., Taam R. E., Zezas A., Bulik T., Maccarone T. J., Ivanova N., 2008, *ApJS*, 174, 223
 Belczynski K., Holz D. E., Bulik T., O’Shaughnessy R., 2016a, *Nature*, 534, 512
 Bethe H. A., Brown G. E., 1998, *ApJ*, 506, 780
 Binney J., Tremaine S., 1987, *Galactic Dynamics*, Princeton University Press, US
 Bird S., Cholis I., Muñoz J. B., Ali-Haïmoud Y., Kamionkowski M., Kovetz E. D., Raccanelli A., Riess A. G., 2016, *Phys. Rev. Lett.*, 116, 201301
 Breen P. G., Hoggie D. C., 2013, *MNRAS*, 432, 2779
 Campanelli M., Lousto C., Zlochower Y., Merritt D., 2007, *ApJ*, 659, L5
 Capuzzo-Dolcetta R., Miocchi P., 2008, *MNRAS*, 388, L69
 Carr B. J., Hawking S. W., 1974, *MNRAS*, 168, 399
 Carr B., Kühnel F., Sandstad M., 2016, *Phys. Rev. D*, 94, 083504
 Chandrasekhar S., 1943, *ApJ*, 97, 255
 Choksi N., Volonteri M., Colpi M., Gnedin O. Y., Li H., 2019, *ApJ*, 873, 100
 Costa G., Bressan A., Mapelli M., Marigo P., Iorio G., Spera M., 2021, *MNRAS*, 501, 4514
 De Luca V., Franciolini G., Pani P., Riotto A., 2021a, *J. Cosmol. Astropart. Phys.*, 2021, 28
 De Luca V., Desjacques V., Franciolini G., Pani P., Riotto A., 2021b, *Phys. Rev. Lett.*, 126, 051101
 de Mink S. E., Mandel I., 2016, *MNRAS*, 460, 3545
 Di Carlo U. N. et al., 2020b, *MNRAS*, 498, 495
 Di Carlo U. N., Giacobbo N., Mapelli M., Pasquato M., Spera M., Wang L., Haardt F., 2019, *MNRAS*, 487, 2947
 Di Carlo U. N., Mapelli M., Bouffanais Y., Giacobbo N., Santoliquido F., Bressan A., Spera M., Haardt F., 2020a, *MNRAS*, 497, 1043
 Doctor Z., Wysocki D., O’Shaughnessy R., Holz D. E., Farr B., 2020, *ApJ*, 893, 35
 Dominik M., Belczynski K., Fryer C., Holz D. E., Berti E., Bulik T., Mandel I., O’Shaughnessy R., 2013, *ApJ*, 779, 72
 Downing J. M. B., Benacquista M. J., Giersz M., Spurzem R., 2010, *MNRAS*, 407, 1946
 du Buisson L. et al., 2020, *MNRAS*, 499, 5941
 Eldridge J. J., Stanway E. R., 2016, *MNRAS*, 462, 3302
 Eldridge J. J., Stanway E. R., Tang P. N., 2019, *MNRAS*, 482, 870
 Farmer R., Renzo M., de Mink S. E., Marchant P., Justham S., 2019, *ApJ*, 887, 53
 Farmer R., Renzo M., de Mink S. E., Fishbach M., Justham S., 2020, *ApJ*, 902, L36
 Farrell E., Groh J. H., Hirschi R., Murphy L., Kaiser E., Ekström S., Georgy C., Meynet G., 2021, *MNRAS*, 502, L40
 Favata M., Hughes S. A., Holz D. E., 2004, *ApJ*, 607, L5
 Fishbach M., Holz D. E., 2020, *ApJ*, 904, L26
 Fishbach M., Holz D. E., Farr B., 2017, *ApJ*, 840, L24
 Fitchett M. J., 1983, *MNRAS*, 203, 1049
 Flitter J., Muñoz J. B., Kovetz E. D., 2020, preprint (arXiv:2008.10389)

- Fragione G., Kocsis B., 2018, *Phys. Rev. Lett.*, 121, 161103
- Fragione G., Loeb A., 2019, *MNRAS*, 486, 4443
- Fragione G., Silk J., 2020, *MNRAS*, 498, 4591
- Fragione G., Ginsburg I., Kocsis B., 2018, *ApJ*, 856, 92
- Fragione G., Loeb A., Rasio F. A., 2020a, *ApJ*, 895, L15
- Fragione G., Loeb A., Rasio F. A., 2020b, *ApJ*, 902, L26
- Fryer C. L., Belczynski K., Wiktorowicz G., Dominik M., Kalogera V., Holz D. E., 2012, *ApJ*, 749, 91
- Gayathri V. et al., 2020, preprint (arXiv:2009.05461)
- Georgiev I. Y., Puzia T. H., Hilker M., Goudfrooij P., 2009a, *MNRAS*, 392, 879
- Georgiev I. Y., Hilker M., Puzia T. H., Goudfrooij P., Baumgardt H., 2009b, *MNRAS*, 396, 1075
- Georgiev I. Y., Böker T., Leigh N., Lützgendorf N., Neumayer N., 2016, *MNRAS*, 457, 2122
- Gerosa D., Berti E., 2017, *Phys. Rev. D*, 95, 124046
- Gerosa D., Berti E., 2019, *Phys. Rev. D*, 100, 041301
- Giacobbo N., Mapelli M., 2018, *MNRAS*, 480, 2011
- Giacobbo N., Mapelli M., Spera M., 2018, *MNRAS*, 474, 2959
- Giersz M., Leigh N., Hypki A., Lützgendorf N., Askar A., 2015, *MNRAS*, 454, 3150
- Goodman J., Hut P., 1993, *ApJ*, 403, 271
- Graham A. W., Spitler L. R., 2009, *MNRAS*, 397, 2148
- Gratton R. G., Fusi Pecci F., Carretta E., Clementini G., Corsi C. E., Lattanzi M., 1997, *ApJ*, 491, 749
- Gratton R. G., Bragaglia A., Carretta E., Clementini G., Desidera S., Grundahl F., Lucatello S., 2003, *A&A*, 408, 529
- Harris W. E., 1996, *AJ*, 112, 1487
- Heggie D. C., 1975, *MNRAS*, 173, 729
- Hills J. G., 1983, *AJ*, 88, 1269
- Hills J. G., Fullerton L. W., 1980, *AJ*, 85, 1281
- Hobbs G., Lorimer D. R., Lyne A. G., Kramer M., 2005, *MNRAS*, 360, 974
- Hofmann F., Barausse E., Rezzolla L., 2016, *ApJ*, 825, L19
- Holley-Bockelmann K., Gültekin K., Shoemaker D., Yunes N., 2008, *ApJ*, 686, 829
- Ji J., Bregman J. N., 2015, *ApJ*, 807, 32
- Jiménez-Forteza X., Keitel D., Husa S., Hannam M., Khan S., Pürrer M., 2017, *Phys. Rev. D*, 95, 064024
- Kimball C. et al., 2020a, preprint (arXiv:2011.05332)
- Kimball C., Talbot C., Berry C. P. L., Carney M., Zevin M., Thrane E., Kalogera V., 2020b, *ApJ*, 900, 177
- Klencki J., Moe M., Gladysz W., Chruslinska M., Holz D. E., Belczynski K., 2018, *A&A*, 619, A77
- Kremer K. et al., 2020, *ApJ*, 903, 45
- Kroupa P., 2001, *MNRAS*, 322, 231
- Kroupa P., Subr L., Jerabkova T., Wang L., 2020, *MNRAS*, 498, 5652
- Kruckow M. U., Tauris T. M., Langer N., Kramer M., Izzard R. G., 2018, *MNRAS*, 481, 1908
- Kumamoto J., Fujii M. S., Tanikawa A., 2019, *MNRAS*, 486, 3942
- Kumamoto J., Fujii M. S., Tanikawa A., 2020, *MNRAS*, 495, 4268
- Kumamoto J., Fujii M. S., Trani A. A., Tanikawa A., 2021, preprint (arXiv:2102.09323)
- Lee H. M., 1995, *MNRAS*, 272, 605
- Liu B., Lai D., 2021, *MNRAS*, 502, 2049
- Lousto C. O., Zlochower Y., 2011, *Phys. Rev. Lett.*, 107, 231102
- Lousto C. O., Zlochower Y., Dotti M., Volonteri M., 2012, *Phys. Rev. D*, 85, 084015
- McKernan B. et al., 2018, *ApJ*, 866, 66
- McKernan B., Ford K. E. S., Lyra W., Perets H. B., 2012, *MNRAS*, 425, 460
- Maggiore M., 2018, *Gravitational Waves: Volume 2: Astrophysics and Cosmology*. Oxford Univ. Press, Oxford
- Mandel I., de Mink S. E., 2016, *MNRAS*, 458, 2634
- Mapelli M., 2016, *MNRAS*, 459, 3432
- Mapelli M., 2018, preprint (arXiv:1809.09130)
- Mapelli M., Giacobbo N., 2018, *MNRAS*, 479, 4391
- Mapelli M., Hayfield T., Mayer L., Wadsley J., 2012, *ApJ*, 749, 168
- Mapelli M., Giacobbo N., Ripamonti E., Spera M., 2017, *MNRAS*, 472, 2422
- Mapelli M., Giacobbo N., Santoliquido F., Artale M. C., 2019, *MNRAS*, 487, 2
- Mapelli M., Santoliquido F., Bouffanais Y., Arca Sedda M., Giacobbo N., Artale M. C., Ballone A., 2020a, preprint (arXiv:2007.15022)
- Mapelli M., Spera M., Montanari E., Limongi M., Chieffi A., Giacobbo N., Bressan A., Bouffanais Y., 2020b, *ApJ*, 888, 76
- Marchant P., Langer N., Podsiadlowski P., Tauris T. M., Moriya T. J., 2016, *A&A*, 588, A50
- Miller M. C., Colbert E. J. M., 2004, *Int. J. Mod. Phys. D*, 13, 1
- Miller M. C., Hamilton D. P., 2002, *MNRAS*, 330, 232
- Miller M. C., Lauburg V. M., 2009a, *ApJ*, 692, 917
- Miller M. C., Lauburg V. M., 2009b, *ApJ*, 692, 917
- Miller M. C., Miller J. M., 2015, *Phys. Rep.*, 548, 1
- Moody K., Sigurdsson S., 2009, *ApJ*, 690, 1370
- Morscher M., Pattabiraman B., Rodriguez C., Rasio F. A., Umbreit S., 2015, *ApJ*, 800, 9
- Neijssel C. J. et al., 2019, *MNRAS*, 490, 3740
- Neumayer N., Seth A., Böker T., 2020, *A&AR*, 28, 4
- Nitz A. H., Capano C. D., 2021, *ApJ*, 907, L9
- Nitz A. H., Dent T., Davies G. S., Harry I., 2020, *ApJ*, 897, 169
- O’Leary R. M., Rasio F. A., Fregeau J. M., Ivanova N., O’Shaughnessy R., 2006, *ApJ*, 637, 937
- O’Leary R. M., Kocsis B., Loeb A., 2009, *MNRAS*, 395, 2127
- O’Leary R. M., Meiron Y., Kocsis B., 2016, *ApJ*, 824, L12
- Özel F., Freire P., 2016, *ARA&A*, 54, 401
- Palmese A., Conselice C. J., 2020, preprint (arXiv:2009.10688)
- Peters P. C., 1964, *Phys. Rev.*, 136, 1224
- Petrovich C., Antonini F., 2017, *ApJ*, 846, 146
- Portegies Zwart S. F., McMillan S. L. W., 2000, *ApJ*, 528, L17
- Portegies Zwart S. F., McMillan S. L. W., 2002, *ApJ*, 576, 899
- Portegies Zwart S. F., Yungelson L. R., 1998, *A&A*, 332, 173
- Portegies Zwart S. F., Baumgardt H., Hut P., Makino J., McMillan S. L. W., 2004, *Nature*, 428, 724
- Portegies Zwart S. F., McMillan S. L. W., Gieles M., 2010, *ARA&A*, 48, 431
- Quinlan G. D., 1996, *New Astron.*, 1, 35
- Quinlan G. D., Shapiro S. L., 1990, *ApJ*, 356, 483
- Rasskazov A., Kocsis B., 2019, *ApJ*, 881, 20
- Renzo M., Farmer R. J., Justham S., de Mink S. E., Göteborg Y., Marchant P., 2020a, *MNRAS*, 493, 4333
- Renzo M., Cantiello M., Metzger B. D., Jiang Y. F., 2020b, *ApJ*, 904, L13
- Rezzolla L., Barausse E., Dorband E. N., Pollney D., Reisswig C., Seiler J., Husa S., 2008, *Phys. Rev. D*, 78, 044002
- Rice J. R., Zhang B., 2021, *ApJ*, 908, 59
- Riley J., Mandel I., Marchant P., Butler E., Nathaniel K., Neijssel C., Shortt S., Vigna-Gomez A., 2020, preprint (arXiv:2010.00002)
- Rizzuto F. P. et al., 2021, *MNRAS*, 501, 5257
- Rodriguez C. L., Morscher M., Pattabiraman B., Chatterjee S., Haster C.-J., Rasio F. A., 2015, *Phys. Rev. Lett.*, 115, 051101
- Rodriguez C. L., Chatterjee S., Rasio F. A., 2016a, *Phys. Rev. D*, 93, 084029
- Rodriguez C. L., Morscher M., Wang L., Chatterjee S., Rasio F. A., Spurzem R., 2016b, *MNRAS*, 463, 2109
- Rodriguez C. L., Amaro-Seoane P., Chatterjee S., Kremer K., Rasio F. A., Samsing J., Ye C. S., Zevin M., 2018, *Phys. Rev. D*, 98, 123005
- Rodriguez C. L., Zevin M., Amaro-Seoane P., Chatterjee S., Kremer K., Rasio F. A., Ye C. S., 2019, *Phys. Rev. D*, 100, 043027
- Romero-Shaw I., Lasky P. D., Thrane E., Calderón Bustillo J., 2020, *ApJ*, 903, L5
- Roupas Z., Kazanas D., 2019, *A&A*, 632, L8
- Safarzadeh M., Haiman Z., 2020, *ApJ*, 903, L21
- Samsing J., 2018, *Phys. Rev. D*, 97, 103014
- Samsing J., Hotokezaka K., 2020, preprint (arXiv:2006.09744)
- Samsing J., MacLeod M., Ramirez-Ruiz E., 2014, *ApJ*, 784, 71
- Sana H. et al., 2012, *Science*, 337, 444
- Santoliquido F., Mapelli M., Giacobbo N., Bouffanais Y., Artale M. C., 2021, *MNRAS*, 502, 4877
- Scelfo G., Bellomo N., Raccanelli A., Matarrese S., Verde L., 2018, *J. Cosmol. Astropart. Phys.*, 9, 039
- Sesana A., Haardt F., Madau P., 2006, *ApJ*, 651, 392

- Spera M., Mapelli M., 2017, *MNRAS*, 470, 4739
- Spera M., Mapelli M., Giacobbo N., Trani A. A., Bressan A., Costa G., 2019, *MNRAS*, 485, 889
- Spitzer L. Jr, 1969, *ApJ*, 158, L139
- Stevenson S., Berry C. P. L., Mandel I., 2017, *MNRAS*, 471, 2801
- Stone N. C., Metzger B. D., Haiman Z., 2017, *MNRAS*, 464, 946
- Tagawa H., Haiman Z., Kocsis B., 2020, *ApJ*, 898, 25
- Tang P. N., Eldridge J. J., Stanway E. R., Bray J. C., 2020, *MNRAS*, 493, L6
- Tanikawa A., Kinugawa T., Yoshida T., Hijikawa K., Umeda H., 2020, preprint ([arXiv:2010.07616](https://arxiv.org/abs/2010.07616))
- Trani A. A., Tanikawa A., Fujii M. S., Leigh N. W. C., Kumamoto J., 2021, *MNRAS*, 504, 910
- Tutukov A., Yungelson L., 1973, *Nauchn. Inf.*, 27, 70
- van Son L. A. C. et al., 2020, *ApJ*, 897, 100
- VandenBerg D. A., Brogaard K., Leaman R., Casagrande L., 2013, *ApJ*, 775, 134
- Venumadhav T., Zackay B., Roulet J., Dai L., Zaldarriaga M., 2020, *Phys. Rev. D*, 101, 083030
- Vigna-Gómez A., Toonen S., Ramirez-Ruiz E., Leigh N. W. C., Riley J., Haster C.-J., 2021, *ApJ*, 907, L19
- Woosley S. E., 2017, *ApJ*, 836, 244
- Woosley S. E., 2019, *ApJ*, 878, 49
- Yang Y., Bartos I., Haiman Z., Kocsis B., Márka Z., Stone N. C., Márka S., 2019, *ApJ*, 876, 122
- Zackay B., Venumadhav T., Dai L., Roulet J., Zaldarriaga M., 2019, *Phys. Rev. D*, 100, 023007
- Zevin M., Samsing J., Rodriguez C., Haster C.-J., Ramirez-Ruiz E., 2019, *ApJ*, 871, 91
- Ziosi B. M., Mapelli M., Branchesi M., Tormen G., 2014, *MNRAS*, 441, 3703

This paper has been typeset from a \LaTeX file prepared by the author.